THESIS FOR THE DEGREE OF LICENTIATE OF ENGINEERING

Comprehensive Description of the Interactions between Silicate Bed Materials and Biomass Ash during DFB gasification

Department of Chemistry and Chemical Engineering

CHALMERS UNIVERSITY OF TECHNOLOGY

Gothenburg, Sweden 2020

Comprehensive Description of the Interactions between Silicate Bed Materials and Biomass Ash during DFB gasification
ROBIN FAUST

Nr 2020:10
Department of Chemistry and Chemical Engineering
Chalmers University of Technology
SE-412 96 Gothenburg
Sweden
Telephone + 46 (0)31-772 1000

Cover:
The cover shows olivine particles after 4 days residence time in the Chalmers gasifier.

Printed by Chalmers Reproservice
Gothenburg, Sweden 2020

Comprehensive Description of the Interactions between Silicate Bed Materials and Biomass Ash during DFB gasification

ROBIN FAUST
Department of Chemistry and Chemical Engineering
Chalmers University of Technology

Abstract

The utilization of biomass for energy generation is a CO_2 neutral alternative to fossil fuel. A suitable way of thermal conversion of biomass is dual fluidized bed (DFB) gasification where biomass is converted to a raw gas which can subsequently be used for chemical synthesis. DFB gasification relies on bed material which functions as a heat carrier to transport thermal energy from the combustor to the gasifier. The bed material's interaction with the inorganic ash fraction released from the biomass can results in detrimental agglomeration which necessitates replacement of the bed material, or beneficial activation which reduces problems associated with unwanted side-products (tar) of the process. Whether agglomeration or activation occurs is dependent on ash composition as well as on the utilized bed material. Different materials have been tested as bed materials for gasification of which three (quartz, olivine, and alkali-feldspar) are the focus of this work. The materials resemble each other in being naturally occurring minerals which are based on silicate networks.

The bed material samples were analyzed with multiple analysis methods after their use in the Chalmers DFB gasifier (such as SEM-EDS, XRD and TEM). The interaction of biomass ash and bed material led to the accumulation of ash-derived elements on the surface of the bed particles. For all three materials, the development of a three layered structure was observed. Common for all materials was that a Mg-rich layer was found on the surface and a Ca-rich layer underneath. The layers between the particles' core and the Ca-rich layer were different for the three materials and is therefore dependent on the utilized bed material. The accumulation of ash-derived elements led to an increase in activity towards tar reduction while at the same time depolymerization of the silicate network of the minerals could be observed.

Acknowledgements

First of all, I want to thank my supervisor Pavleta Knutsson for her guidance and support, and for all the scientific and non-scientific discussion, which always enriched my day. I also would like to thank Martin Seemann for helping me to think about my results from a different point of view.

Thanks to every former and current part of the Cinder group for always providing a welcome platform for fruitful discussions.

I would also like to thank all my co-authors, who taught me many things about gasification, bed materials and sample analysis.

Furthermore, I want to thank everyone at OOMK for making fika and lunch welcome breaks. Special thanks to my office mates Vedad and Julien for helping me with matlab and always reminding me that life is to be enjoyed.

I also would like to thank my family for their moral support. Finally, thanks to Marie for always believing in me.

List of Publications

Paper I

Role of K and Ca for catalytic activation of bed material during biomass gasification

Robin Faust, Jelena Maric, Teresa Berdugo Vilches, Britt-Marie Steenari, Martin Seemann, Pavleta Knutsson

23rd International Conference on Fluidized Bed Conversion (2018), Seoul

Paper II

Layer Formation on Feldspar Bed Particles during Indirect Gasification of Wood – Part 1 K-feldspar

Robin Faust, Thomas Karl Hannl, Teresa Berdugo Vilches, Matthias Kuba, Marcus Öhman, Martin Seemann, Pavleta Knutsson

Energy & Fuels (2019), 33, 7321-7332

Paper III

Layer Formation on Feldspar Bed Particles during Indirect Gasification of Wood – Part 2 Na-feldspar

Thomas Karl Hannl, Robin Faust, Matthias Kuba, Pavleta Knutsson, Teresa Berdugo Vilches, Martin Seemann, Marcus Öhman

Energy & Fuels (2019), 33, 7333-7346

Paper IV

Microscopic investigation of layer growth during olivine bed material aging during indirect gasification of biomass

Robin Faust, Mohammad Sattari, Jelena Maric, Martin Seemann, Pavleta Knutsson

Fuel (2020), 266, 117076

Paper V

Comparison of Ash Layer Formation Mechanisms on Si-containing Bed Material during Dual Fluidized Bed Gasification of Woody Biomass

Robin Faust, Teresa Berdugo Vilches, Per Malmberg, Pavleta Knutsson

Submitted for peer-review to Energy & Fuels

Contents

1 Introduction

The world total primary energy supply 2017 was about 14000 Mtoe (about 590 EJ).[1] The sources to feed this energy demand were to more than 80% fossil fuels (oil, coal and natural gas).[1] Anthropogenic greenhouse gas emissions (GHG) have continuously increased from 1970 to 2010.[2] CO_2 emitted by fossil fuel combustion reached 32 $GtCO_2$/year in 2010 which makes up almost 80% of the total emissions.[2] The figure for total emissions has increased to 36 $GtCO_2$/year until 2017 (Figure 1.1).[3] According to the IPCC, these emissions are expected to further increase if no counter measures are realized. Compared to pre-industrial levels, this would lead to an increase in mean surface temperature of between 3.7 °C and 4.8 °C by the end of the 21st century.[2]

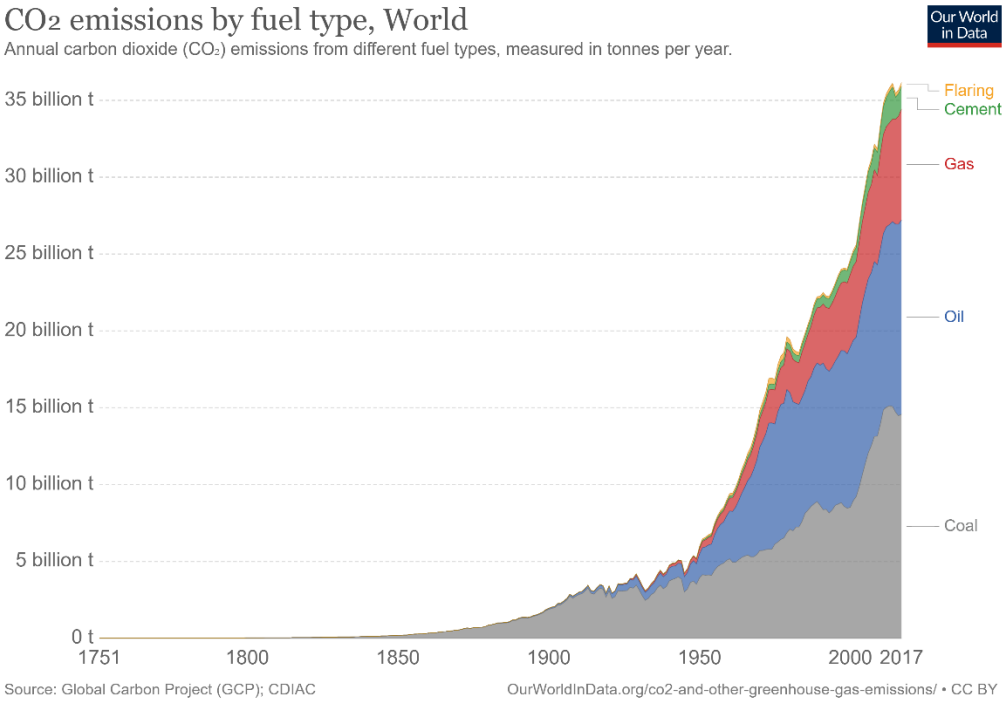

Figure 1.1: Global CO_2 emissions by fuel type (1751-2017).[3]

Several counter measures, so-called mitigation options, are listed in the IPCC report, one of which is the implementation of bioenergy.[2] The utilization of biomass as feedstock for energy generation presents a renewable alternative towards fossil fuels.[4–6] Biomass includes organic matter which is derived from plants or animals.[7] During its growth, plant-based biomass consumes CO_2 from the atmosphere which is subsequently released back during combustion. Thus, in biomass combustion the net emissions of CO_2 is zero, which is why biomass can be considered a CO_2 neutral feedstock.[5–7] Conversion of biomass instead of coal presents therefore a sustainable alternative to fossil fuels. The overall technical energy potential of biomass was calculated to be in the range of 50 – 500 EJ by 2050.

Even though it is considered that the CO_2 released by biomass combustion is taken up by the growing biomass, the time interval between release of CO_2 and the re-absorption heavily depends on the type of biomass utilized.[8,9] When assessing the CO_2 emissions resulting from biomass conversion, it is therefore not sufficient to assume all biomass as CO_2 neutral. Furthermore, the applicability of biomass must also be considered regarding socio-economic factors such as food supply, and environmental issues such as the

loss of biodiversity caused by industrial biomass plantations.[10] Accounting for the latter two arguments, the utilization of forestry residues or woody biomass acquired from afforestation of degraded land, has the greatest benefit on atmospheric CO_2 levels, as these solutions do not contribute to the loss of biodiversity or threaten our food supply.[2,9] Forest residues from logging and processing alone were estimated to be 28 EJ/year.[11] Additionally, plantations of fast-growing plant species such as miscanthus or sugar cane present opportunities of shorter carbon emission and sequestration cycles.[2] The total potential of utilizing marginal and degraded land for dedicated biomass plantations was estimated to be about 100 EJ.[12,13] This number could be further increased, if growing genetically modified plants is considered possible, where the plants' ability to perform photosynthesis is improved.[14,15]

Besides biomass, carbonaceous feedstock from waste streams can be utilized for energy generation, such as municipal solid waste,[16] sewage sludge[17] or plastic.[18] A major challenge with biomass and waste streams is their non-homogeneous composition, regarding both organic and inorganic compounds. This requires flexibility of operational parameters to reach the optimal conditions for thermal conversion of each particular type of feedstock. An efficient and flexible technology for thermal conversion of heterogeneous fuels is dual fluidized bed (DFB) gasification.[19]

2 Gasification

Gasification is a process where a carbonaceous feedstock is thermally converted to CO, H_2 and CO_2. This is realized by applying high temperatures and limiting the available oxygen to avoid complete combustion. For the reaction to occur, a reducing gas is applied, such as H_2O or CO_2. The carbonaceous feedstock, denoted simply as C, is then converted according to reactions 1a and 1b.

$$C + H_2O + heat \rightarrow CO + H_2 \quad (1a)$$

$$C + CO_2 + heat \rightarrow 2\ CO \quad (1b)$$

$$C + O_2 \rightarrow CO_2 + heat \quad (2)$$

Both reactions are endothermic which means that thermal energy needs to be supplied. This can be done by combusting a part of the fuel, for example by supplying air to the reactor (reaction 2). The heat released by the combustion can then be utilized for the gasification reaction. The gas created this way is however diluted with O_2 and N_2 which are introduced by the air. This means the gas is of lower calorific value and therefore less valuable. To avoid the dilution, the two processes (combustion and gasification) can be locally separated from each other, as done in dual fluidized bed (DFB) gasification.

2.1 Dual Fluidized Bed (DFB) Gasification

The technology of DFB gasification is based on two fluidized bed reactors (see Figure 2.1).[20,21] In the combustor, fuel is converted in an exothermic reaction to heat and flue gas. Inside the combustion reactor (combustor), bed material consisting of small (about 100-300 µm) mineral particles, is fluidized by an oxygen-containing gas stream. The heat emitted by the oxidation of the fuel is taken up by the bed material which is transported to the gasifier by the circulating fluidized bed material. In the gasifier, the endothermic gasification reaction takes place which converts fuel to raw gas. In order for the bed material to sustain the process, the bed material needs to withstand thermal and mechanical stress which are associated with the process. During the process, loss of material cannot be completely avoided which is why economic factors such as availability and low disposal costs need to be taken into account when selecting bed material.[22]

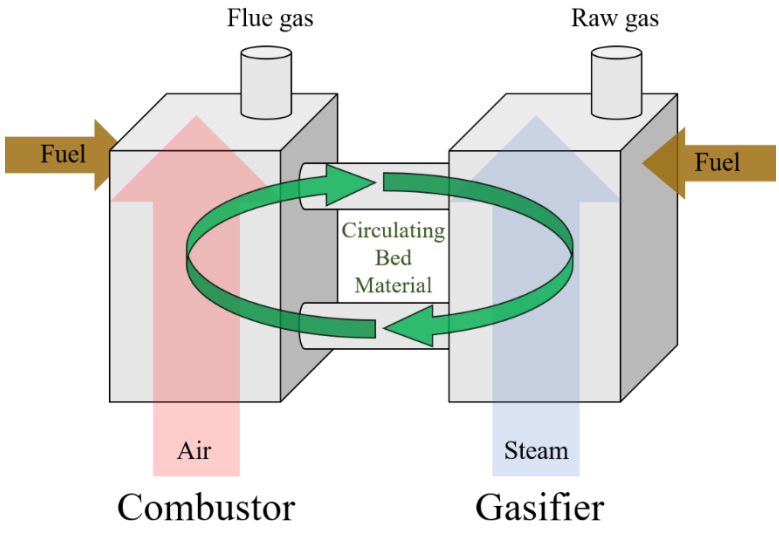

Figure 2.1: Simplified illustration of the working principle of a DFB gasifier. In the combustor, fuel is converted in an exothermic reaction. The heat is transported by fluidized bed material to the gasifier, where the endothermic gasification reaction converts the fuel to raw gas.

The produced raw gas contains mainly CO, CO_2, H_2, H_2O, CH_4 but also other hydrocarbons. This gas can be further purified for H_2 production or processed into a precursor for biofuel or other chemicals.[5,23] An important parameter for the gas quality is the concentration and composition of the hydrocarbons (heavier than CH_4) in the produced gas. Especially the generation of tar, which is the group of larger polyaromatic hydrocarbons, (such as benzene, toluene and naphthalene) poses a problem to the gasification process.[24,25] Tar tends to condensate on downstream equipment, where they cause problems such as clogging which often requires unplanned shut-downs of the process.[26,27] Furthermore, as chemical energy is stored in their bonds, tars represent a loss of energy in the raw gas. The formation of tars has therefore been identified as the most critical problem during biomass gasification.[23,26–29] While a number of different materials fulfill the previously mentioned requirements, major research efforts have been made to minimize the formation of tars, where the application of catalytically active bed material has proven to be an effective strategy.[25,30–33] Several naturally occurring minerals have been tested as bed material, such as quartz, olivine, dolomite, feldspar, bauxite, ilmenite, as well as mixtures of them.[17,31–36]

2.2 Silicate Minerals

The majority of the mineral matter found in the earth's crust are silicate based minerals. As these minerals are abundant and cheap and at the same time attrition resistant, they present suitable candidates for the application as bed material. Silicate (SiO_4^{4-}) is an anion present as tetrahedrons (one Si^{4+} in the center and four O^{2-} in the corners), which is the building blocks of many different minerals. Depending on the composition of the minerals, the charge is balanced by the incorporation of cations or by polymerization of the silicate tetrahedrons into larger corner-sharing structures. The degree of polymerization of the silicate tetrahedrons is the basis for classification of the multitude of silicate-based minerals into several sub-groups (see Figure 2.2).

At low concentrations of silicon, the silicate tetrahedrons are present as isolated islands (Figure 2.2a). Minerals based on isolated silicate island are therefore called nesosilicates (after Greek 'nesos' for island). The residual charge of the silicate anions is balanced by interstitial cations. One of the most prominent members of this group is olivine which is a magnesium iron silicate ($(Mg, Fe)_2SiO_4$). Olivine exhibits a

high crystallization temperature which is why it is one of the first minerals to crystallize upon cooling of basaltic magma. The concentration of Si in olivine is lower than in basaltic magma, which is why the magma becomes enriched in Si. Higher concentrations of Si reduce the crystallization temperature of the magma and necessitate the formation of corner-sharing silicate chains (Figure 2.2b), so called inosilicates (after Greek 'inos' for fiber). The crystallization of inosilicates further enriches the magma in silicate, which leads to the formation of double-chain-silicates, sheet-silicates and finally tectosilicates. Quartz (SiO_2) is the final product of cooling magma and exhibits a tectosilicate structure (Figure 2.2c). While pure quartz has a high melting point, small impurities as present in cooling magma decrease the crystallization temperature to 600 – 700 °C. Due to aluminum present in the magma, Ca-rich plagioclase is formed at the same temperatures as olivine, and alkali feldspar at the crystallization temperature of quartz. As it is the first product of cooling magma, olivine is most abundant in the earth's mantle and the ocean floor whereas quartz and alkali-feldspar are components of the continental crust. One important property of quartz is its resistance to chemical weathering which is why it can be found as sand on beaches, and therefore facilitates its application as bed material.

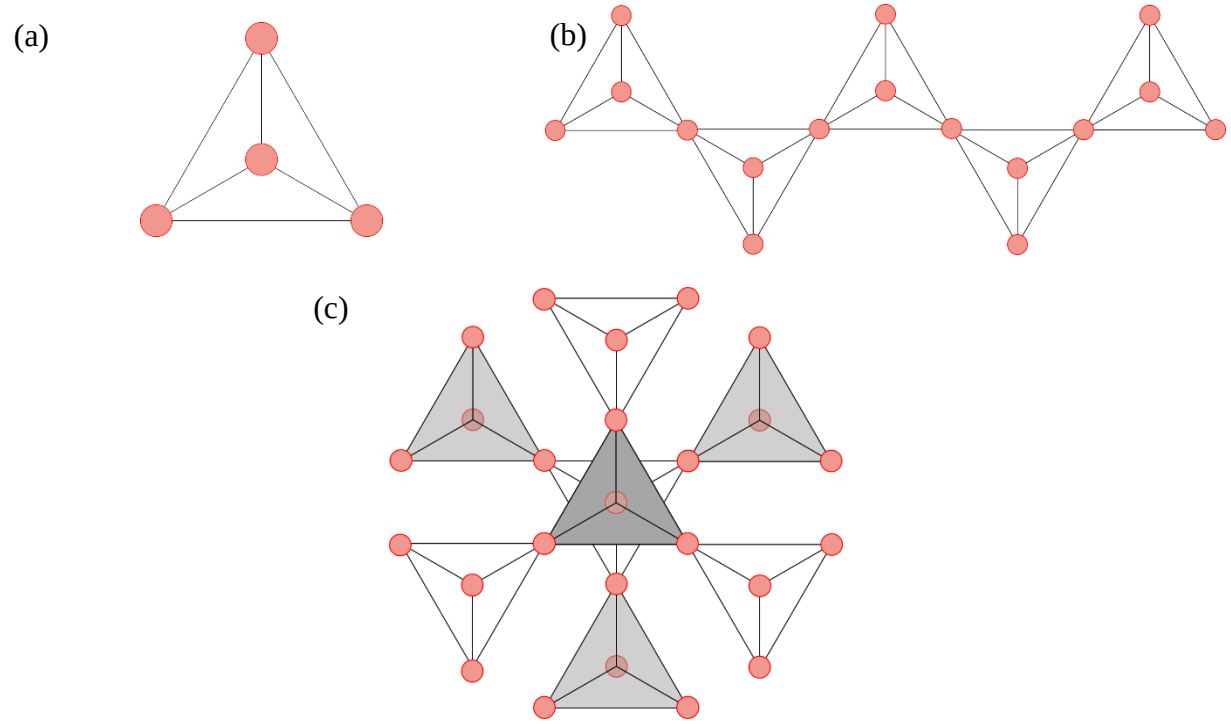

Figure 2.2: Schematic depiction of the silicate framework present in many minerals. (a) nesosilicate, (b) inosilicate, (c) tectosilicate.

2.3 Biomass Ash

When thermally converting biomass to raw gas, apart from the organic fraction that is converted to raw gas, the inorganic fraction of the feedstock also needs to be taken into consideration (see Figure 2.3). The inorganic fraction represents the unconvertable share of biomass, often denoted simply as ash. A part of the formed ash remains in the system and can react with the material surfaces present in the reactor (e.g. bed material, refractories). The composition of the formed ash is dependent on the utilized feedstock. While fast-growing grass species exhibit high amounts of silicon, the major components of woody biomass ash are potassium and calcium.[37,38] Other elements commonly found in biomass ash are magnesium, sodium, aluminum, iron, sulfur and phosphorous.[39]

The presence of ash forming species in the gasifier and their interaction with the bed material particles can have both detrimental and beneficial influence on the process. The ash elements can accumulate in the bed particles which can cause them to stick together. This leads to the formation of bigger particle aggregates, often referred to as agglomerates, that eventually leads to loss of fluidization (defluidization). On the other hand, the presence of ash compounds on the particles' surface can improve the previously mentioned catalytic activity of the bed material. Besides ash composition of the used fuel, the decisive factor for either of these effects to occur is the bed material itself.

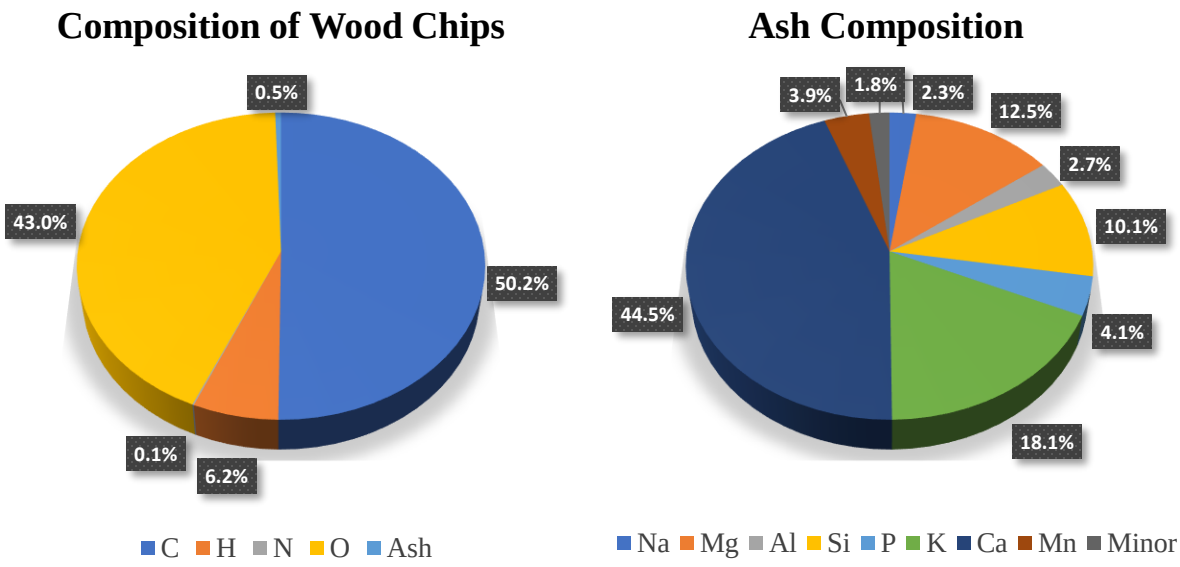

Figure 2.3: Composition of (spruce and pine) wood chips (wt. %) utilized in the present study and the ash composition (mol %).

A critical parameter for the choice of bed material is therefore the interaction of the bed material with biomass ash.[22] This interaction has been the focus of a number of studies to investigate under which circumstances detrimental agglomeration or beneficial catalytic activation occurs. Berdugo Vilches[40] investigated the activity of different bed materials over prolonged retention time by measuring the yield of naphthalene, which is a tar species commonly formed during gasification and thus a suitable indicator for the bed material activity (see Figure 2.4). The figure shows a decreasing trend for the olivine and feldspar, whereas prolonged retention time of silica sand is not suitable as the material is prone to agglomerate.

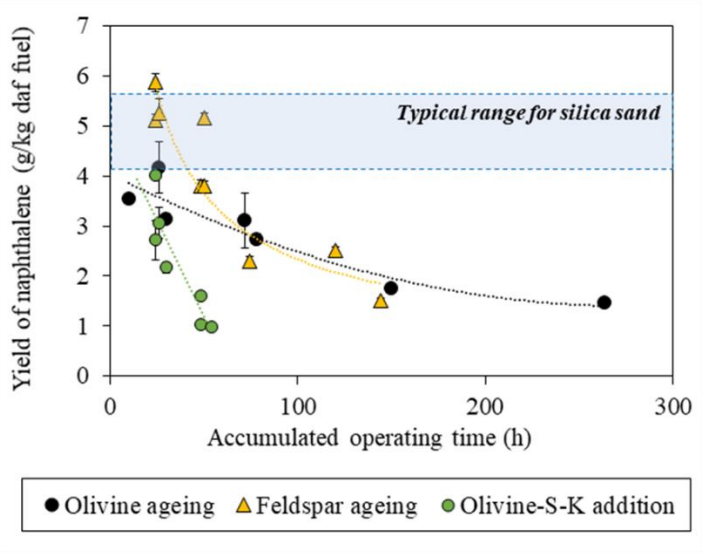

Figure 2.4: Naphthalene yield for different bed materials used for biomass gasification in the Chalmers DFB gasifier. Prolonged operating time is not suitable for silica sand due to agglomeration. Reprinted with permission from Berdugo Vilches.[40]

2.4 Agglomeration

Agglomeration describes the process of bed material particles sticking together to larger clusters. This hampers bed pressure and can in the worst case lead to defluidization of the bed material. The severity of agglomeration related problems depends on the choice of bed material and the composition of biomass ash and their interaction.

In the literature, three different mechanisms are described causing agglomeration of bed material, which are schematically shown in Figure 2.5.[41–44] Agglomeration caused by melt deposition (Figure 2.5a) is typical for biomass which is inherently rich in K and Si. Biomass rich in K and Si can therefore lead to agglomeration regardless of the bed material applied. If biomass rich in K is used, the interaction with the bed material is to be taken into consideration. K can be released from the biomass as gaseous KOH which can interact with the bed material, as the mechanism shown in Figure 2.5b. The interaction of $KOH_{(g)}$ with the bed material can lead to the formation of low melting K-silicates which can cause agglomeration. Furthermore, the deposition of ash elements to form a coating can cause agglomeration, as the interaction of the coating layer with the bed particle can lead to low melting phases (Figure 2.5c).[41–43]

Alkali silicates which exhibit low melting temperatures, have generally been identified as the determining species to cause agglomeration.[45,46] This can be explained from a thermodynamic point of view as shown in Figure 2.6. While pure quartz exhibits a melting point of close to 2000 K, any addition of K_2O (or Na_2O) leads to the formation of melt. Thus, especially the combination of quartz sand and biomass yielding ash rich in alkali metals, has been reported to cause defluidization of the bed material.[41,45–50] Therefore, alternative bed materials have been successfully applied, which are significantly less vulnerable to agglomeration than quartz, such as olivine, feldspar and dolomite.[36,45,47,50] Alternatively, the addition of kaolin or Al_2O_3 as a substance to bind alkali metals released from the ash has shown beneficial results, as the formation of low-melting alkali silicates is avoided.[49,51] Generally, the knowledge of the interaction

between biomass ash and bed material can aid to choose suitable combinations of bed material, biomass, and additives to prevent or delay agglomeration related problems.

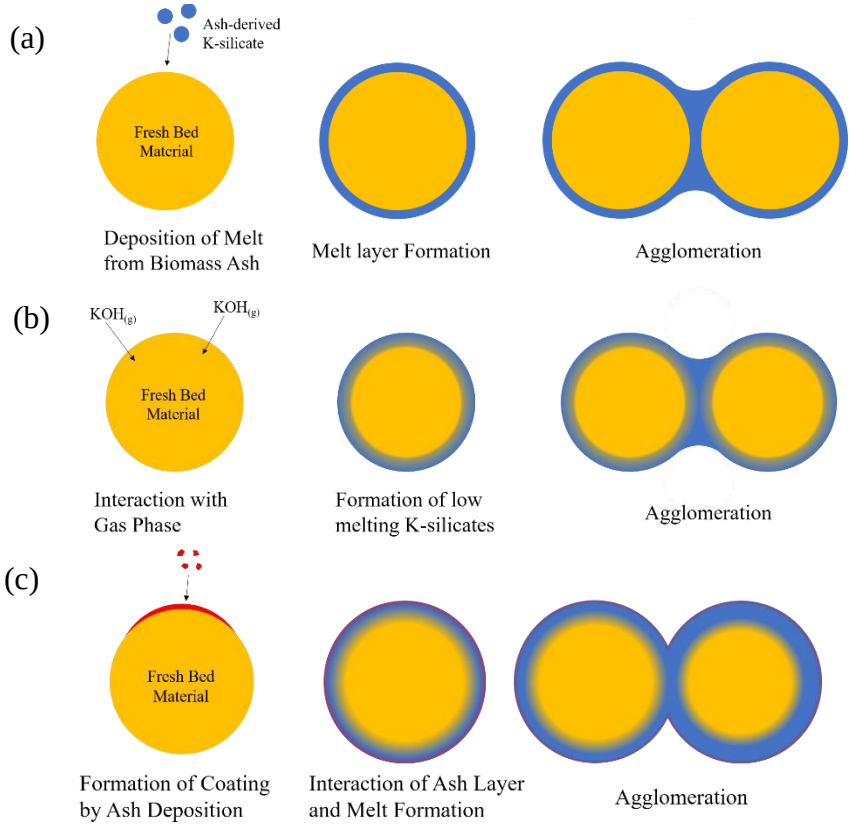

Figure 2.5: Schematic depiction of different agglomeration mechanisms. (a) agglomeration caused by melt deposition, (b) agglomeration caused by melt formation due to interaction with gaseous K, (c) agglomeration caused by the interaction of the coating layer with the bed particle.

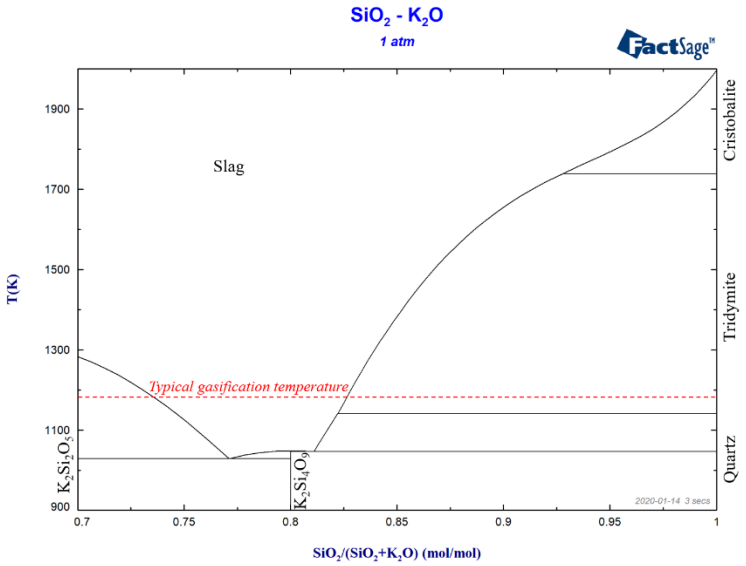

Figure 2.6: Phase diagram of SiO_2 and K_2O of the SiO_2-rich side at 1 atm. For low concentrations of K_2O, the region corresponds to tridymite and slag (melt). The share of melt increases with increasing K_2O concentration until pure melt is expected at around 18 % K_2O.[52]

2.5 Activation

2.5.1 Quartz

Besides being available, cheap, and easy to dispose, quartz has sufficiently strong mechanical stability and can function as a heat carrier for DFB gasification. However, high amounts of tars are formed in the product gas when quartz is used as bed material. Furthermore, the previously described agglomeration due to the interaction with ash-derived potassium is most severe for the case of quartz and causes defluidization and therefore unplanned stops of the process.[41,42]

The accumulation of ash-derived calcium on the surface of the quartz particles has shown increase in activity towards tar reduction.[33] However, this effect is overshadowed by the agglomeration which necessitates bed material replacement. Due to the increased risk for agglomerate formation with time, prolonged retention time of the quartz particles in the gasification system, which would be necessary for the activation, is not practical.

2.5.2 Olivine

Olivine has been successfully utilized as bed material for biomass gasification, as it, similarly to sand, fulfills the criteria for bed material. Additionally to the mechanical stability and heat transfer, olivine has shown catalytic activity towards tar reduction.[26,31,53] In multiple studies it was further observed that the activity of olivine could be improved by calcination of the particles prior to application, an effect that was explained by accumulation of iron on the particles' surface.[34]

Moreover, the interaction of biomass ash with olivine was shown to further enhance the activity of the material. By prolonged retention time (aging) of the particles in the gasification system the tar concentration in the product gas could be gradually decreased.[54] The increased activity with time spent in the gasifier could be explained by the formation of a layer rich in ash derived elements, such as potassium and calcium.

The mechanism of layer formation and its effect on the tar concentration has been the topic of extensive research.[30,55–60] It was found that the interaction of ash elements with olivine does not lead to agglomeration associated problems (as was previously observed in the case of quartz sand), as the uptake of potassium into the olivine structure is minor compared to that in quartz.[60] Instead of the formation of low-temperature melting potassium silicates, the formation of calcium silicate by a replacement of magnesium and iron from the olivine lattice was reported.[60] Furthermore, the location of potassium was found to be decisive for the activity of the material. When located close to the surface, potassium could enhance the activity, but due to migration towards the particles' cores, it was no longer available at the surface and the material became deactivated.[59]

Even though considered as promising bed material, due to the demonstrated activity towards tars, one major drawback of olivine are the elements nickel and chromium which are often naturally incorporated into the mineral olivine.[54,61] The presence of these heavy metals requires special treatment of the bed material after its removal from the gasifier (material fraction referred to as bottom ash).[50] Alkali-feldspar was therefore tested as an alternative to olivine bed material.

2.5.3 Feldspar

Feldspar is mechanically stable and the most abundant mineral in earth's crust, making it cheap and readily available and thus a suitable bed material. Furthermore, due to the absence of hazardous heavy metals in the natural minerals, no special attention needs to be taken when disposing the waste material.

Alkali-feldspar has been successfully applied as bed material for biomass gasification.[36,62,63] It has been shown that the interaction of feldspar with biomass ash does not cause major problems with agglomeration, instead activation (as found for olivine) was reported.[62,63] Again, this was associated with the formation of layers rich in ash elements.[62,64] In a study on K-feldspar used for combustion of woody biomass, the mechanism for the layer formation was described as a substitution of K^+ by ash-derived Ca^{2+}-ions. This led to the formation of cracks after prolonged retention time of the particles. The reaction with alkaline species on the other hand, was found to be low.[64]

2.6 Objective

The objective of this work was to comprehensively describe the mechanism of ash layer formation for different silicate-based bed materials, by applying a novel sample preparation method. It was further attempted to find similarities regarding layer formation for the three different materials in order to predict the bed material's response to changes in process parameters such as fuel composition, temperature, or presence of additives. As the surface of the bed particles is in contact with the gas phase and therefore responsible for tar cracking, the knowledge of elemental and crystallographic composition of the bed material's surface layer can aid to take advantage of the effect of activation while at the same time avoiding detrimental agglomeration.

3 Experimental

To study the interaction of bed material and biomass ash during DFB gasification, several studies were conducted which are summarized in Figure 3.1. The different experiments are described in more detail in the following sections. The morphology and composition of the bed particles was analyzed with several different techniques to study the changes in the bed material induced by its interaction with biomass ash.

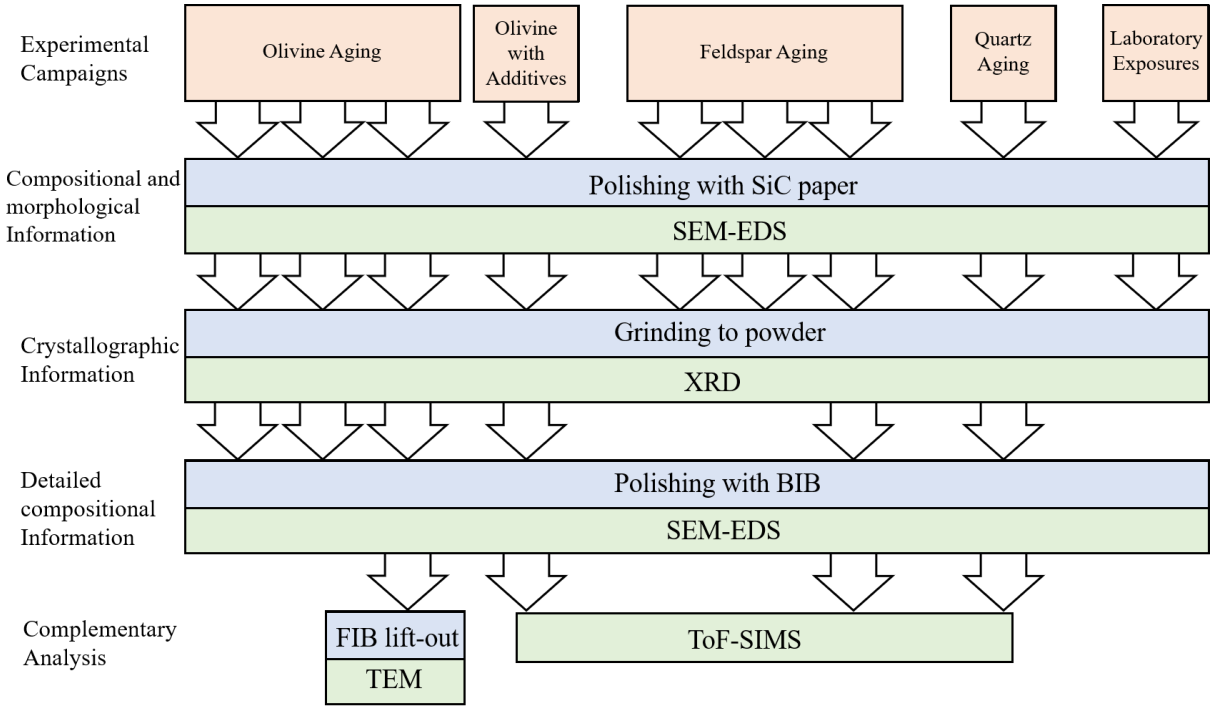

Figure 3.1: Experimental campaigns and analysis conducted over the course of this work. The experiments conducted are shown in red, sample preparation in blue and sample analysis in green.

3.1 Bed Materials and Feedstock

Three different bed materials were tested and investigated as bed materials in the Chalmers DFB gasifier – quartz, olivine, and feldspar. Their composition, as provided by the suppliers, is shown in Table 1. All three materials contain a major amount of Si. Despite being a natural material, the quartz utilized is of high purity with only small contaminations with Al and Fe. Olivine contains mostly Mg, Fe and Si and the ratio between Mg and Fe to Si is slightly lower than 2:1 which would be the case for pure olivine. As mentioned earlier, olivine contains small amounts of nickel and chromium. The feldspar utilized is a mixture of 40 weight percent (wt. %) Na-feldspar, 48 wt. % K-feldspar, 6 wt. % Ca-feldspar and 6 wt. % quartz. The majority of the particles of all materials was between 180 and 500 µm.

Wood chips and wood pellets were used as fuel for the combustor and the gasifier accordingly. Both feedstocks have relatively low content of ash – 0.5 wt. % (wood chips) and 0.4 wt. % (wood pellets) ash, respectively. The ash composition of the feedstocks is shown in Table 2. As it can be read from the table, in both cases, calcium and potassium constitute the major ash components, followed by magnesium and silicon.

Table 1: Elemental composition of the bed materials studied in the present thesis, as provided by the material suppliers on an oxygen-free basis.

mol %	Quartz	Olivine	Feldspar
Na			7.56
Mg		60.48	0.05
Al	0.20	0.44	20.10
Si	99.76	34.11	61.25
P			0.06
K			9.72
Ca			1.17
Ti			0.01
Cr		0.20	
Fe	0.04	4.55	0.08
Ni		0.21	

Table 2: Ash composition of the utilized feedstocks. Wood chips were fed to the combustor and wood pellets to the gasifier.

	Wood Chips [mmol/kg]	Wood Pellets [mmol/kg]
Na	1.3	2.2
Mg	7.0	9.1
Al	1.5	0.7
Si	5.7	2.8
P	2.3	3.2
K	10.2	21.0
Ca	25.0	32.4
Ti	<0.2	<0.2
Mn	2.2	1.1
Fe	0.7	0.4
Ba	0.1	0.1

3.2 Sample Exposures

The first four experimental campaigns shown in Figure 3.1 were exposed in the Chalmers DFB gasifier. The system consists of a 12 MW_{th} circulating fluidized bed (CFB) furnace and a 2-4 MW_{th} bubbling fluidized bed (BFB) gasifier. A schematic representation of the plant is shown in Figure 3.2. The bed material is heated up in the furnace (1) where wood chips are combusted with air used as fluidization gas. The bed material particles are separated from the fine fraction in the gas by the cyclone (4) and transported by the particle distributor (9) to the gasifier (11). The gasifier has a separate fuel feeding system, where wood pellets are used as feedstock. From the gasifier, bed material and remaining unconverted char are transported back to the furnace. To avoid gas leakage, loop seals, which are fluidized with steam, are placed in between the cyclone and the gasifier, and between the gasifier and the furnace. A detailed description of the system can be found elsewhere.[19]

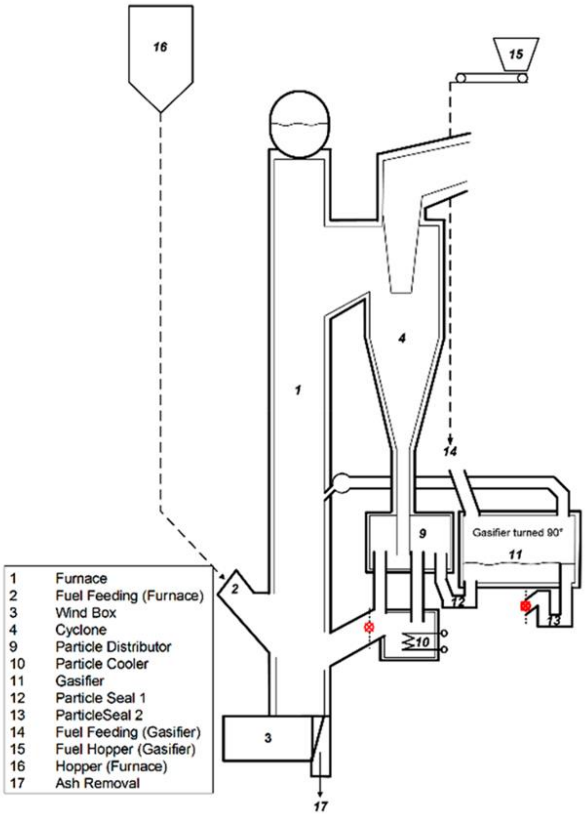

Figure 3.2: Schematic representation of the Chalmers Dual Fluidized Bed (DFB) gasifier.[19]

Each of the bed materials described earlier (quartz, olivine, and feldspar), was utilized in an aging experiment, which is conducted for a prolonged time without bed material regeneration or additives. Thereby, the time-resolved interaction of bed material and ash could be studied. In another campaign, olivine was utilized, and ammonium sulfate was added to control CO emissions. The exact experimental parameters can be found in the respective publications (on quartz,[22] olivine,[54] feldspar[36] and olivine with additives[18]). The prolonged retention time of the particles in the system lead to an increase in tar cracking ability of the material in all cases (see Figure 2.4).

The system of biomass ash is complex as it contains a myriad of elements which interact with the bed material. Studying the effect of single elements separately, is therefore difficult, as other ash-derived elements might overshadow these effects. This is why the system was further simplified to study the diffusion of potassium and calcium. Therefore, a laboratory set-up was applied where flat olivine stones were placed into a tubular furnace under oxidizing conditions at 850 °C for 24 hours. Slurries of K_2CO_3, K_2SO_4, $CaCO_3$ and $CaCl_2$, which are salts of the major biomass ash elements, were placed onto them to study the interactions with each of the salts separately.

3.3 Sample Preparation and Analysis

3.3.1 SEM-EDS

To analyze the influence of biomass ash and additives on the bed material, particles were investigated with a scanning electron microscope (SEM). The particles were mounted on a conductive carbon tape onto a SEM-stub and information about the morphology was acquired by recording micrographs. Thereby, surface properties such as porosity could be investigated. However, especially the formation of layers caused by the interaction of biomass ash and bed material is of relevance for activation or agglomeration. Therefore, cross-sections of the particles were prepared which necessitates the immobilization of the bed material particles. This was achieved by two different methods.

In the first method, a mixture of resin and hardener was used for embedding of the bed material particles. After curing, the samples could be ground and polished with SiC paper (until P2400). To avoid dissolution of the alkali salts during preparation, this was done without cooling agent. By this method, a great number of particles (several hundreds) could be immobilized simultaneously which was useful for preliminary material analysis as well as for statistical analysis. This method is widely used within the field and gives a good understanding of the materials. However, when grinding material with different mechanical properties, such as particles and their layers, the mechanically weaker part gets ground quicker which can cause damage in the ash layer and hamper the analysis. Furthermore, by mechanical grinding one is limited in the final surface quality that can be achieved.

In order to overcome the enumerated limitations, a second sample preparation method was developed. Small amounts of sample particles were embedded between two silicon wafers with cyanoacrylate glue. After curing, the “sandwich” was mounted in a broad ion beam (BIB) system. The process is schematically shown in Figure 3.3. The lower part of the sandwich was protected from the beam with a mask and only the topmost few millimeters were removed by the beam. Thereby, cross-sections of a small number of particles were created at the same time and a surface finish with a higher quality was obtained.

A direct comparison of the two sample preparation methods can be seen in Figure 3.4. The figure shows two olivine particles from the same sample which has been exposed to biomass ash for 24 hours in the Chalmers gasifier. From the image it is visible, that only by the second method, sufficient surface quality can be achieved for further analysis of the ash layer. This is especially important for the early layer formation, where the ash layer is too thin to be analyzed otherwise.

Furthermore, by utilizing energy dispersive X-ray spectroscopy (EDS), information about the elemental composition was acquired. Thereby, the distribution of ash-derived elements throughout the surface layer of the particles can be followed. By studying the composition throughout the ash-layers, conclusions can be made on whether agglomeration is likely to occur or if tar-reduction can be attributed to the elemental composition on the particles’ surface. While measuring the composition is useful to derive which elements are involved in activation of the bed material, no crystallographic information can be acquired by SEM-EDS.

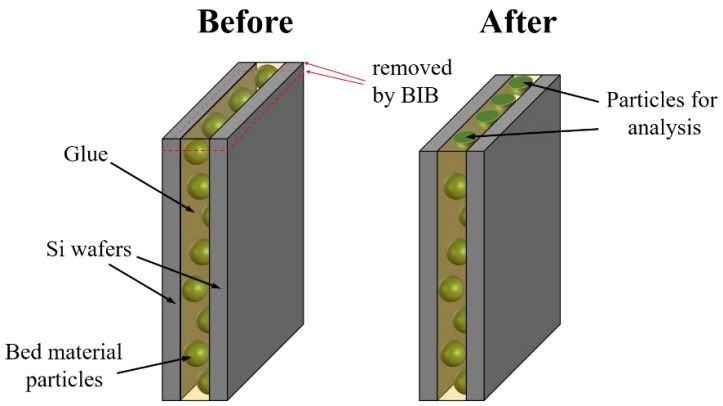

Figure 3.3: Schematic representation of the cross-section sample preparation method with broad ion beam (BIB) milling. The particles were embedded between two silicon wafers with cyanoacrylate glue and subsequently the topmost part was removed by BIB-milling. Thereby, cross-sections of a few particles were created.

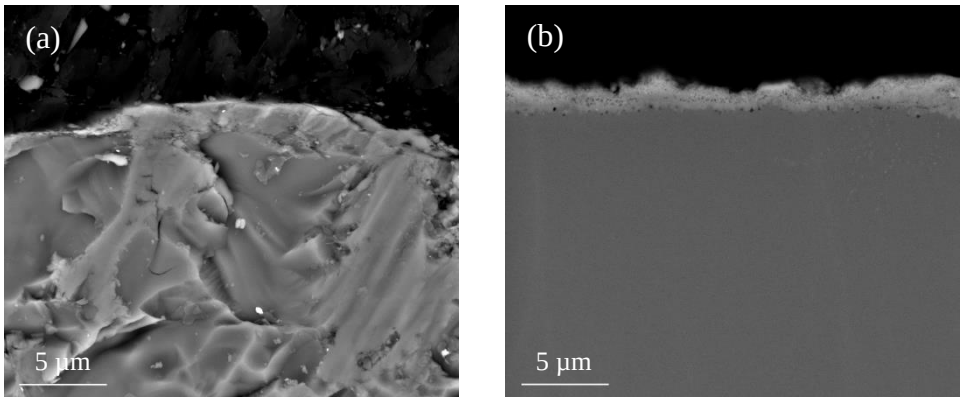

Figure 3.4: SEM-micrographs of an olivine sample, which was exposed to biomass ash for 24 hours, illustrating the two different sample preparation methods. (a): grinding with SiC paper; (b): BIB-milling.

3.3.2 X-Ray Diffraction (XRD)

The crystallographic phases were analyzed by X-ray diffraction (XRD). The samples were ground to a fine powder prior to analysis to improve the statistical distribution of the crystallites. The recorded spectra were compared qualitatively to the patterns from databases. Together with the data from SEM-EDS, information on the phases present on the particles' surface could be acquired. These phases are most likely in contact with the gas phase, where the breakdown of tar species occurs and are therefore the reason for the bed material's activity. However, XRD analysis provides crystallographic information from the whole particle which can make it difficult to analyze the development of the layer formation. The signal stemming from the phases which are formed on the surface of the bed material particles is weak, compared to the rest of the bed material. It can therefore become challenging to precisely identify minor phases formed during the interaction.

3.3.3 Transmission Electron Microscopy (TEM)

For the purpose of higher resolution analysis, a lift-out (about 6 µm x 10 µm) of a sample was created by focused ion beam (FIB) milling using gallium ions. The sample was polished down to a thickness of about 100 nm until it was sufficiently thin for electrons to pass through, to be analyzed by transmission electron microscopy (TEM). This process requires multiple sample preparation steps making it time-consuming and expensive. Furthermore, only a small part of the surface of one particle can be analyzed which could make

it questionable whether the sample is representative of the whole bed material in the gasifier. It is therefore crucial to conduct the previously described analysis (SEM-EDS and XRD) beforehand and to carefully select a representative location of the particle. Once the representativity of the sample was ensured, TEM could be used for high-resolution imaging, elemental analysis (TEM-EDS) and to obtain crystallographic information by TEM-diffraction.

3.3.4 Additional Analysis

Complementary to the listed techniques, a number of other analysis techniques were applied. To study the effect of K in surface vicinity, which is likely to positively influence the tar cracking ability of the bed material, extracted bed material particles were immersed in water to leech out soluble species. The concentration of soluble K^+ was analyzed with atomic absorption spectroscopy (AAS). Furthermore, since the amount of surface area of the bed material available to the gas phase could influence the catalytic tar cracking reactions, Brunauer-Emmett-Teller (BET) analysis were conducted. Lastly, the elemental distribution of bed material cross-sections was investigated by time of flight secondary ion mass spectroscopy (ToF-SIMS) to investigate whether molecular-ions could be found. This information was used complementary to XRD to derive the nearest neighbors of elements found in the active layers.

3.4 Thermodynamic Modelling

Complementary to the experimental results, thermodynamic modelling offers theoretical information on the layer development. Therefore, FactSage was used to calculate the inorganic phases which are stable at the conditions present in the gasification system. The calculations are based on minimizing the Gibbs energy which results in information on the phases which are thermodynamically stable, without accounting for the process kinetics. The elemental compositions found with SEM-EDS were used as input data (as their respective oxides) and the calculations could be used to investigate melting behavior and to support the results found with XRD. Furthermore, by studying possible reactions, the mechanism of the interaction between bed material and biomass ash compounds could be derived.

4 Results & Discussion

Three different bed materials (quartz, olivine, and feldspar) were investigated in the course of this work, regarding their interaction with woody biomass ash derived elements. The materials were sampled during different experimental campaigns conducted in the Chalmers gasifier. The interactions were studied by the analysis techniques described before and their results compared to thermodynamic calculations.

4.1 Morphology

The interaction of bed material with biomass ash leads to change in morphology of the bed particles. This can be seen from top-view micrographs as recorded on olivine and feldspar particles with different retention times (see Figure 4.1). The surface changes from exhibiting sharp edges at the beginning of the experiments towards more smooth features towards later extraction times. This can be attributed to both attrition and accumulation of ash elements. For the case of feldspar, cracking of the surface layer can be detected, as indicated with the arrows in Figure 4.1 (e) and (f).

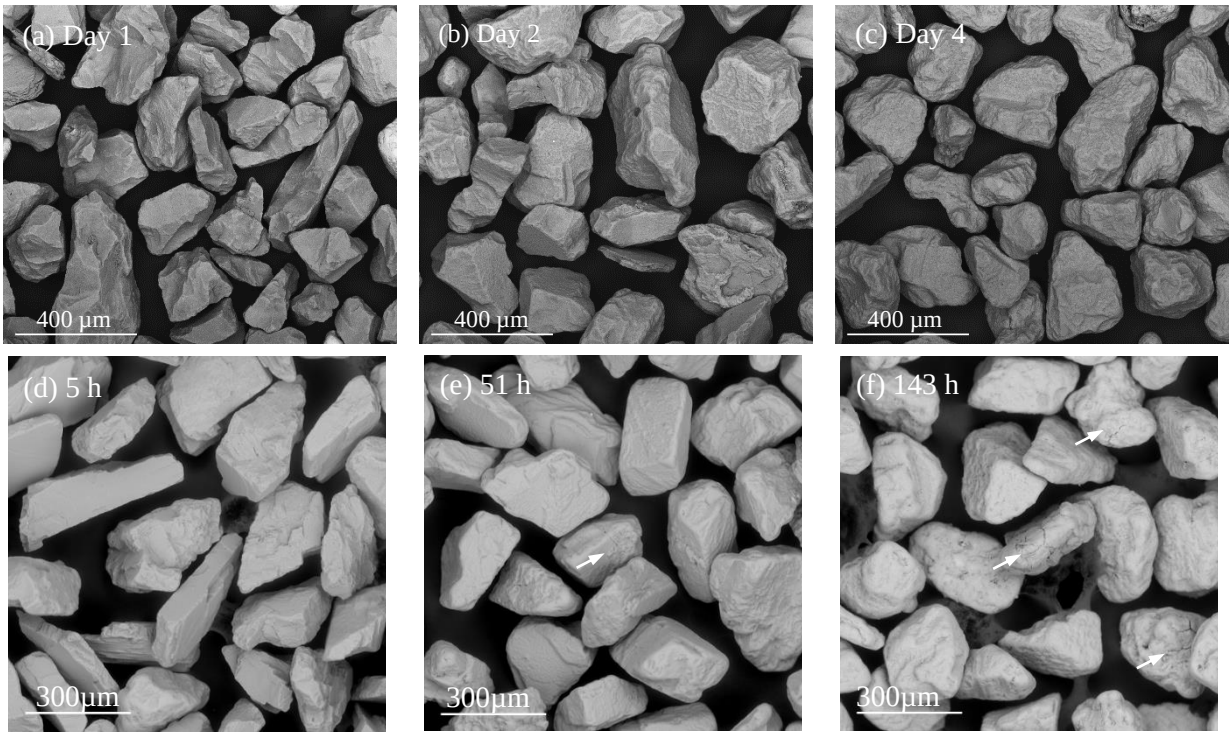

Figure 4.1: Top-view SEM micrographs of the olivine particles (a-c) and feldspar particles (d-f) exposed in aging experimental campaigns in the Chalmers gasifier. Cracking of the ash layer is indicated with arrows.

Cross-sections of the particles extracted from the olivine aging experimental campaign are shown in Figure 4.4. The figure shows the formation of a layer brighter in back-scattered electron (BSE) contrast after 1 day retention time with an increase in its thickness after 2 and 4 days. A brighter BSE contrast corresponds to the presence of elements heavier than those originally present in olivine (Mg, Si and O). This is true for Ca and K which are major biomass ash elements. The formation of a brighter layer can therefore be interpreted as an accumulation of ash elements on the surface of the bed particles.

The same was found for quartz and feldspar as shown in Figure 4.2. The figure shows the development of the ash layer of quartz, olivine, and alkali-feldspar after three days. As can be seen in the figure, in all cases the particles are covered by a brighter layer. The thickness varies between the different materials and the layer is most pronounced for quartz and to a lesser extent olivine. The feldspar particle exhibits less accumulation of ash elements than the other materials and the resulting ash layer is significantly thinner after similar exposure times.

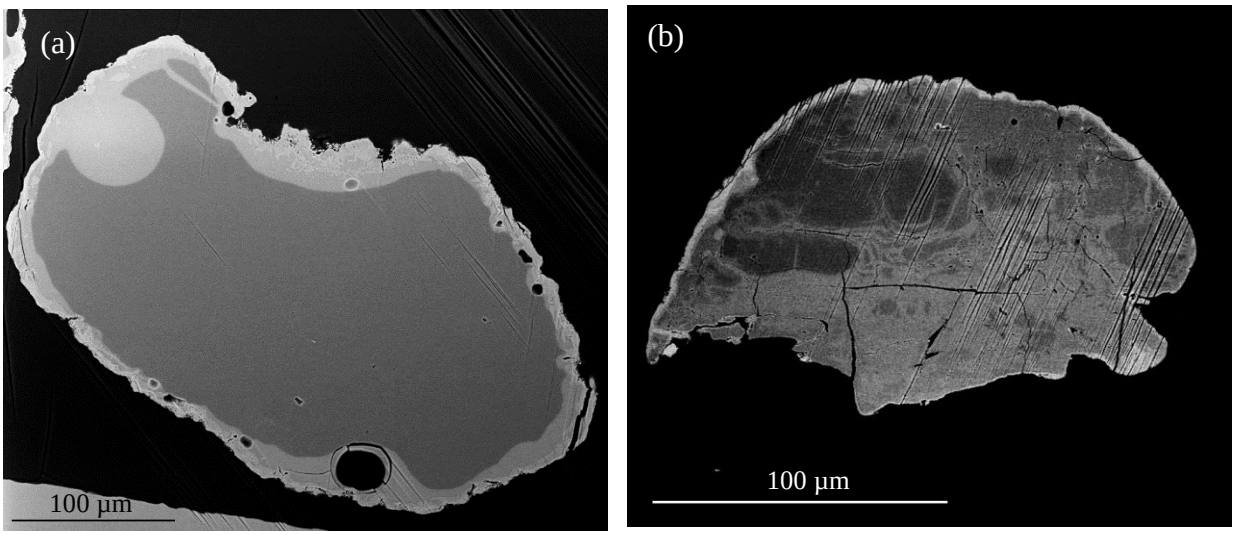

Figure 4.2: SEM micrograph of a cross-section of quartz and feldspar particles used as bed material. Formation of surface layers rich in ash elements is visible for quartz (a) and feldspar (b) after 3 days interaction with biomass ash in the Chalmers DFB gasifier.

While the core of quartz and olivine particles is largely unaffected by prolonged exposure time in the gasifier, a change in BSE contrast for the core can be observed for alkali-feldspar particles investigated in the aging experiment (see Figure 4.3). After 5 hours in the gasifier, the contrast difference between darker Na-rich feldspar (indicated as α) and the brighter K-rich feldspar (indicated as β) is clearly visible. After 51 hours, however, the amount of darker Na-rich feldspar has significantly decreased. In the sample extracted after 143 hours, only at the center of a few particles the darker contrast corresponding to Na-feldspar can be found.

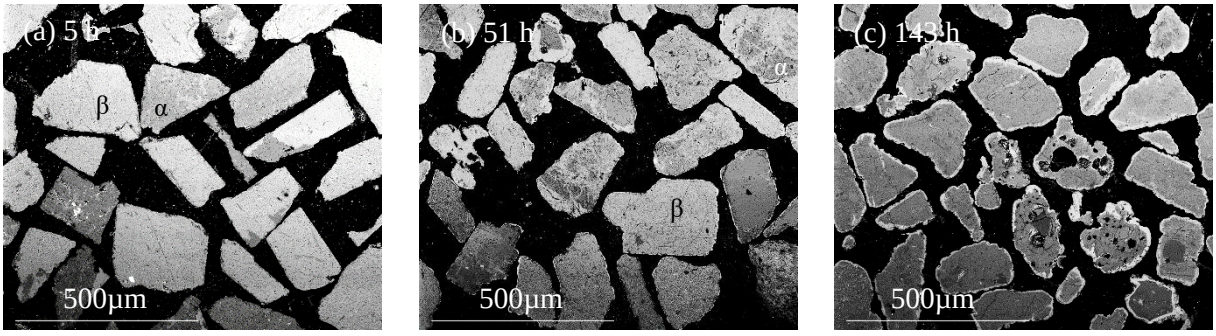

Figure 4.3: BSE mode SEM micrographs of cross-sections of alkali-feldspar particles exposed in the aging experimental campaign, extracted after different retention times. The contrast corresponding to Na-feldspar and K-feldspar is indicated with α and β, respectively.

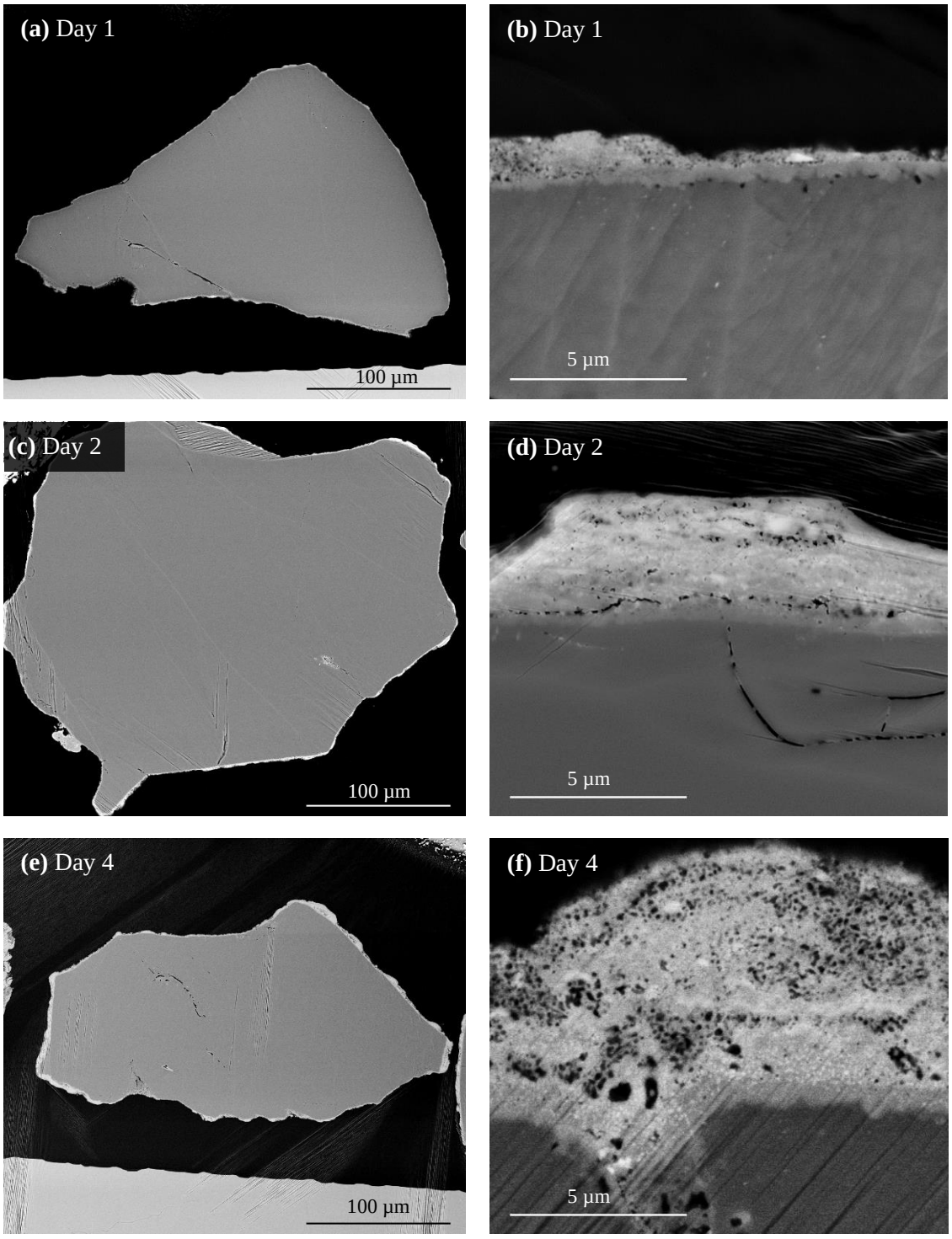

Figure 4.4:BSE mode SEM micrographs of cross-sections of particles extracted from the Chalmers gasifier after 1, 2 and 4 days of retention time without bed material replacement or addition of additives.

4.2 Layer Structure

To study the formation and composition of the ash layers, EDS line-scans were recorded on micrographs (see Figure 4.5). The samples shown had been in the gasifier for 3 days and the goal was to compare the layer formation mechanism for the three materials. The formation of three distinct layers could be found for all materials investigated, where the highest Mg concentration was found on the surface, the highest Ca concentration further inside the layer, and finally a primary interaction layer between bed material and biomass ash at the interface between particle center and the Ca-rich layer. The specific layer formation characteristics for each material are discussed in the following sections separately.

4.2.1 Quartz

The particle shown in Figure 4.5 (a) is covered by a uniform layer of between 10 and 50 µm thickness. From the micrograph this layer can be divided into three sublayers.

The *surface layer* which comprises the outer 2-3 µm of the particles is slightly brighter in contrast and contains high amounts of ash elements, distributed as 15 at. % Mg, 40 at. % Ca and 10 at. % P. Compared to other locations in the sample, the concentration of Si (30 at. %) is particularly low on the surface. Furthermore, the *surface layer* exhibits a large number of small pores.

The *intermediate layer* can be distinguished by the presence of rather defined edges and extends for about 5-10 µm into the particles. The characteristic presence of such geometrical shapes indicates the growth of crystallites from a melt. The *intermediate layer* contains a higher amount of Si and K (about 50 at. % and 10 at. % respectively) compared to the *surface layer*, whereas the concentration of Ca within this layer is lower (30 at. %). Neither Mg, nor P cannot be found in significant amounts. No porosity can be detected in the *intermediate layer*.

The *inner layer* can be characterized by a high concentration of K and Si (up to 20 and 70 at. % respectively) and a very smooth layer morphology which is interrupted by voids (bubbles) of several micrometer in diameter. The morphology indicates that this area was in a molten state while the particles were present in the gasifier. This is supported by the previously suggested growth of crystallites into the melt. The concentration of Ca is much lower here compared to the *intermediate layer*.

4.2.2 Olivine

Figure 4.5 (b) shows the layer formed on an olivine particle during the experimental campaign where potassium carbonate and ammonium sulfate were added to the process. One can distinguish two separate layers from the BSE contrast, one dense inner layer and one more porous outer layer. The thickness of the dense layer stays rather constant, whereas the outer layer increases in thickness to up to 10 µm which is unevenly distributed throughout the particle. Within the outer layer, several spots of brighter contrast can be observed which indicate the formation of a separate phase which is mostly located on the surface of the outer layer. One can therefore once again distinguish three separate layers.

The *surface layer* is the area which is brighter in BSE contrast. From the EDS line-scan shown in Figure 4.5 (e), one can conclude that this area is rich in Mg and comparably poor in Si. Underneath is the *intermediate layer* which is rich in ash derived elements such as Ca and P. As mentioned previously, a high amount of porosity can be found here. The coincidence of Ca and P indicates the formation of calcium phosphate. The *inner layer* is rich in Ca, Mg and Si. Its morphology does not exhibit any pores, and it appears to be homogeneous in BSE contrast.

The interaction of K with olivine is of particular interest due to the catalytic activity associated with K. Compared to quartz, the interaction with olivine is minor and significantly less K is accumulated in the bed material. This explains why olivine does not tend to agglomerate even when K_2CO_3 is added to the process and instead the bed material increases in activity.[59] From the EDS line-scan one can observe the coincidence of K and S in the *surface* layer, which indicates the formation of K_2SO_4. In the study where no ammonium sulfate was added, the presence of K could not be found in the surface layer which suggests, that the addition of sulfate provides a binding partner for K.

4.2.3 **Feldspar**

The sample extracted after three days retention time was prepared with the BIB-milling method and a K-rich feldspar particle is shown in Figure 4.5 (c). From the BSE contrast one can observe the formation of two layers. The EDS line-scan shows a maximum in Na-concentration at the location corresponding to the darker, lower part of the layer. On the surface of the layer, the highest Mg concentration can be observed, and the Ca concentration is highest underneath. Thus, once again three layers can be described, a Mg-rich *surface layer*, a Ca-rich *intermediate layer*, and a Na-rich *inner layer*. Si can be found throughout the whole area. Since the amount of Na in biomass ash is minor, the presence of significant amounts of Na on the particles' surface layer requires a diffusion of Na towards the surface. This can proceed by replacing Na from the feldspar structure by K. This further explains the previously mentioned contrast differences that disappeared with time between the particles (see Figure 4.3), where all Na-rich feldspar has been converted to K-rich feldspar.

The study on originally Na-rich feldspar particles showed similar layer formation, a Mg-rich layer on the surface, followed by a Ca-rich layer. Additionally, the formation of a third layer in between Ca-rich layer and the bulk was found. This layer was denoted as a K-reaction layer, as the concentration of K was higher in this layer than in the bulk and the two layers closer to the surface. This observation is in line with the suggested replacement of Na from the feldspar structure by the ash-derived K.

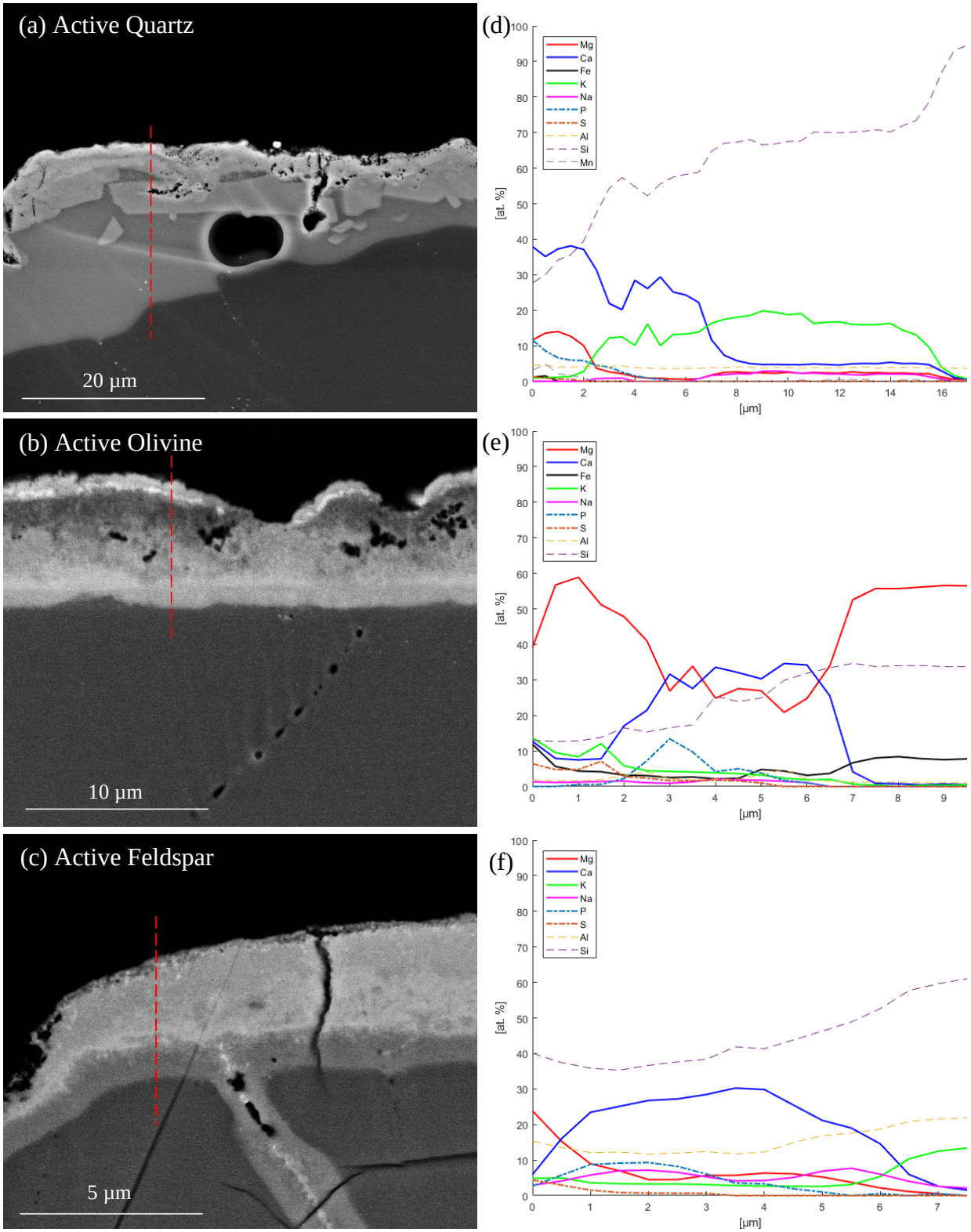

Figure 4.5: BSE (SEM) micrograph and corresponding EDS line-scan of quartz, olivine and feldspar after 3 days retention time in the Chalmers DFB gasifier.

4.3 Crystallography

4.3.1 Quartz

To investigate which crystallographic phases are present in the sample, XRD was performed on the active quartz particles, as well as on fresh ones used as a reference (see Table 3). No phases except for SiO_2 could be found in the fresh sample. After three days of interaction with biomass ash, trace amounts of $CaSiO_3$ (wollastonite), $CaMg(SiO_3)_2$ (diopside) and $Ca_3Mg(SiO_4)_2$ (merwinite) could be found. This indicates the incorporation of Ca^{2+} and Mg^{2+} into the silicate lattice which leads to a depolymerization of the silicate structure. As mentioned before, the quartz structure consists of corner sharing silicate tetrahedrons, whereas in wollastonite and diopside only two out of four oxygens are shared with adjacent tetrahedrons, forming a silicate chain. In merwinite, each silicate tetrahedron is an island, surrounded by divalent cations which means that no oxygen is shared.

As Mg is primarily found on the surface of the exposed quartz sample, merwinite is expected to be located at these locations. The concentration of Si increases towards the center of the particle which is why diopside is most likely located adjacent to merwinite. Together they make up what was previously described as the *surface layer*. The *intermediate layer* which does not contain any Mg but a larger concentration of Ca, is therefore expected to consist of wollastonite. Despite being the thickest layer, no phase which exhibits a high concentration of K, corresponding to the *inner layer* could be found with XRD. While this could be due to the high detection limit of the technique (5 wt. %), it can be also explained by the lack of crystallinity of the layer. Thus, the absence of a phase in XRD, corresponding to the inner layer, supports the previously speculated hypothesis on melt formation. When the particles are extracted from the gasifier, they are quenched which could prohibit crystallization of the melt, forcing it to form an amorphous glass structure.

*Table 3: XRD analysis of quartz before and after exposure in the Chalmers gasifier. The crystallographic phases and their respective silicate structure are shown. The abundance of the phases is indicated with stars: *** - major, ** - minor, * - trace.*

Phase		Silicate-structure	Quartz	
			Fresh	Active
SiO_2	Quartz	tecto	***	***
$CaSiO_3$	Wollastonite	chain		*
$CaMg(SiO_3)_2$	Diopside	chain		*
$Ca_3Mg(SiO_4)_2$	Merwinite	island		*

4.3.2 Olivine

The change of crystallographic phases between the different samples was investigated with XRD and the results are shown in Table 4. It can be seen that the fresh olivine contains low amounts of $MgSiO_3$ (enstatite), which explains the higher content of Si in the fresh material (Table 1) than expected for pure olivine.

The sample extracted after one day of aging shows a decrease in the intensity of the enstatite peak. However, quartz was also present in this sample which could be explained by contamination of the sample with bed material from previous experimental campaigns, as quartz is not expected to form during the interaction of olivine with biomass ash. After two days of retention time, Ca-rich phases can be detected with XRD, such as $CaMgSiO_4$ (monticellite) and $Ca_3Mg(SiO_4)_2$ (merwinite). At the same time MgO (periclase) can be found. This trend continues towards the sample obtained after four days, where the peaks corresponding to monticellite, merwinite and periclase increase in intensity. Similar observations could be made for the

sample collected after application of additives. Here, Ca_2SiO_4 (larnite) could be found, as well as K_2SO_4, which had been predicted from the SEM-EDS results.

*Table 4: XRD results from the different olivine samples investigated. The abundance of the phases is indicated with stars: *** - major, ** - minor, * - trace.*

Phase		Silicate-structure	Olivine				S-K-Addition
			Fresh	Day 1	Day 2	Day 4	
$(Mg,Fe)_2SiO_4$	Olivine	island	***	***	***	***	***
$MgSiO_3$	Enstatite	chain	**	*	*		*
SiO_2	Quartz	tecto		**			
$CaMgSiO_4$	Monticellite	island			*	**	*
$Ca_3Mg(SiO_4)_2$	Merwinite	island			*	**	*
Ca_2SiO_4	Larnite	island					*
MgO	Periclase				**	**	**
K_2SO_4							*

The depolymerization of the silicate lattice, as described for quartz, could be confirmed for the case of olivine, albeit to a lesser extent, as the olivine structure already consists of depolymerized silicate island. However, the previously mentioned trend can be confirmed by following the disappearance of the peak corresponding to enstatite, which exhibits silicate chains. These chains can depolymerize due to the interaction with ash-derived Ca. The interaction of CaO with olivine causes the formation of Ca-Mg silicates which necessitates the displacement of Mg which therefore forms a separate MgO phase, according to the reaction scheme (Figure 4.6).

$$2\ Mg_2SiO_4 \xrightarrow{+\ 2\ CaO} 2\ CaMgSiO_4 + 2\ MgO \xrightarrow{+\ CaO} Ca_3Mg(SiO_4)_2 + MgO \xrightarrow{+\ CaO} 2\ Ca_2SiO_4 + MgO$$

Figure 4.6: Reaction scheme for the interaction of olivine with CaO, leading to the formation of MgO and different Ca-Mg silicates.

4.3.3 **Feldspar**

The XRD results of the experimental campaign with alkali-feldspar are shown in Table 5. It could be seen that the peak corresponding to Na-feldspar (albite) decreases significantly in intensity throughout the exposure, which can be explained by the previously described replacement of Na in the feldspar structure by K. Furthermore, the presence of $CaSiO_3$ (wollastonite) was found, which corresponds to the Ca-rich *intermediate layer*. As Mg-containing phases, $MgSiO_3$ (enstatite) and $Ca_3Mg(SiO_4)_2$ (merwinite) were found, which are expected to be present in the *surface layer*.

Similar to the case of quartz, depolymerization of the silicate structure was found, from a tecto-silicate structure as in feldspar, to a chain-silicate, as in wollastonite or enstatite, to finally an island-silicate, as in merwinite.

*Table 5: Crystallographic phases found with XRD in the samples obtained from the feldpsar aging experiment. The abundance of the phases is indicated with stars: *** - major, ** - minor, * - trace.*

Phase		Silicate-structure	Feldspar fresh	5h	21h	51h	76h	143h
$KAlSi_3O_8$	Microcline	tecto	***	***	***	***	***	***
$NaAlSi_3O_8$	Albite	tecto	***	**	**	**	**	*
$(Na,K)AlSiO_4$	Nepheline	tecto				*	*	*
$CaSiO_3$	Wollastonite	chain			*	**	**	***
$MgSiO_3$	Enstatite	chain					*	*
$Ca_3Mg(SiO_4)_2$	Merwinite	island					*	**

4.4 Thermodynamic Modelling

Equilibrium calculations (Equilib) with FactSage 7.2 were conducted with the compositions acquired from the EDS line-scan (Figure 4.5). The concentration of elements found with EDS were used as input values in their respective fully oxidized form. The calculated phases which are in equilibrium for the measured compositions are shown in the following chapters.

4.4.1 Quartz

The calculations shown in Figure 4.7 are to a large extent in agreement with the previous results. According to the performed calculations, the *inner layer* is composed of a melt. The *intermediate layer* which exhibits a high concentration of Ca, was calculated to consist mostly of $CaSiO_3$. However, the *surface layer*, which is rich in Mg, was found to contain $CaMgSi_2O_6$ and $Ca_2MgSi_2O_7$ which are more polymerized silicate structures than the suggested merwinite.

Besides the silicates, $Ca_3P_2O_8$ was found as the stable P-containing phase. This can be interpreted as the presence of P in the ash reduces the amount of Ca which can react with the silicate structure, as it causes the formation of stable calcium phosphate.

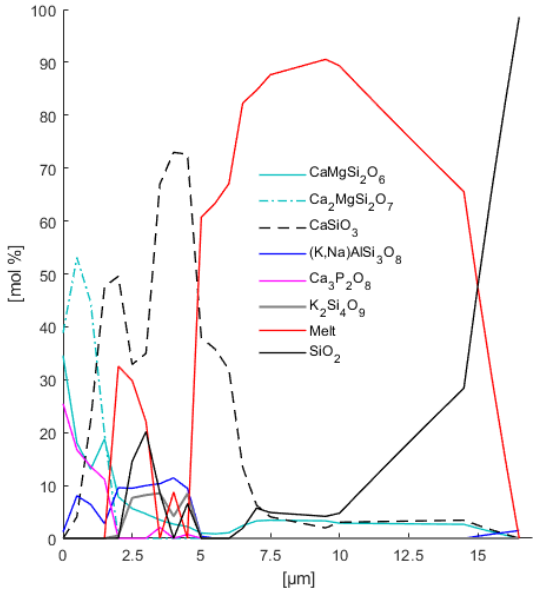

Figure 4.7: Thermodynamic modelling results using FactSage, showing the predominant phases formed if an equilibrium is assumed for the compositions measured with EDS.

Furthermore, FactSage was utilized to develop a reaction mechanism for the interaction of quartz with K_2O and CaO which is shown in Figure 4.8. It has been concluded from the EDS data that the reaction of quartz (SiO_2) and K occurs first, forming a melt. Indeed, the reaction of K_2O with SiO_2 leads to the formation of $K_2Si_4O_9$ which has a melting temperature of 771 °C, well below the usual temperature for biomass gasification (850 °C). The interaction of this melt with CaO leads to the formation of $CaSiO_3$, which depletes the melt of SiO_2. This eventually leads to the formation of K-silicates with higher melting temperatures. As no such K-silicates were found with XRD, it is expected that they can react again with quartz, forming the low melting $K_2Si_4O_9$.

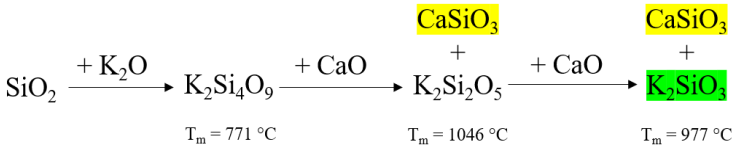

Figure 4.8: Reaction mechanism (as suggested by thermodynamic calculations using FactSage) for the interaction of quartz with oxides of the major ash elements, K_2O and CaO. The melting temperatures (T_m) of the K-silicates are shown.

4.4.2 **Olivine**

As detected with XRD, the phase stable for the composition of the *surface layer* is MgO and in the *intermediate layer*, $Ca_3Mg(SiO_4)_2$ was calculated (see Figure 4.9). $CaMgSiO_4$ and Mg_2SiO_4 form a solid solution (olivine) and are summarized as one phase (Mg_2SiO_4), which is present at the location of the *inner layer*. Minor amounts of melt formation were predicted by FactSage, mostly present in the *intermediate layer*. Any P found with EDS was calculated to form $Ca_3P_2O_4$, effectively removing Ca from the interaction with the silicate structure by the formation of a stable calcium phosphate. The coincidence of K and S was calculated to be due to the formation of K_2SO_4.

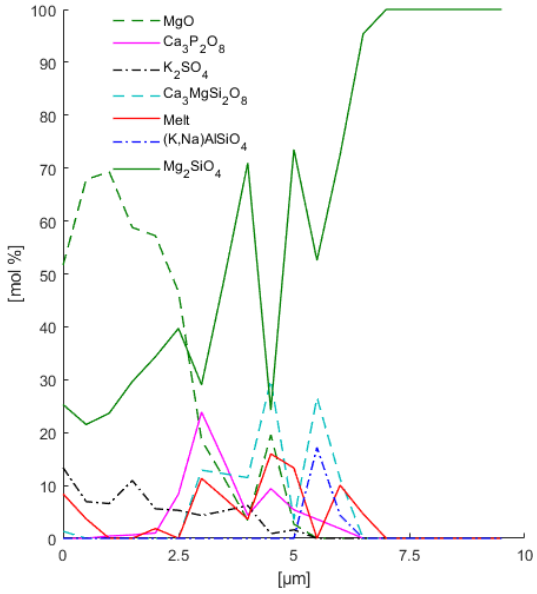

Figure 4.9: FactSage thermodynamic modelling results showing the predominant phases which are in equilibrium for the compositions measured with EDS.

4.4.3 **Feldspar**

According to the calculations (see Figure 4.10), the core of the particle consists of feldspar and quartz. The two different feldspar types (Na-rich and K-rich) are present in a solid feldspar solution at the present temperature. In the figure they are therefore added together and denoted as one phase ($KAlSi_3O_8$). The presence of quartz was calculated, as the concentration of Si was higher than pure feldspar. In the adjacent *inner layer* and *intermediate layer*, the concentration of feldspar decreases, and $CaSiO_3$ is the most abundant phase. The reaction of CaO with feldspar to $CaSiO_3$ requires the depletion of Si from feldspar which is why the feldspathoids leucite ($KAlSi_2O_6$) and nepheline ($(Na,K)AlSiO_4$ are expected from thermodynamic calculations. Additionally, $CaMgSi_2O_6$ was calculated as the Mg-containing phase. As the concentration of Si decreases towards the *surface layer*, the island-silicate Mg_2SiO_4 was calculated to be present here. As was found previously for the case of quartz and olivine, $Ca_3P_2O_8$ is the P-containing stable phase.

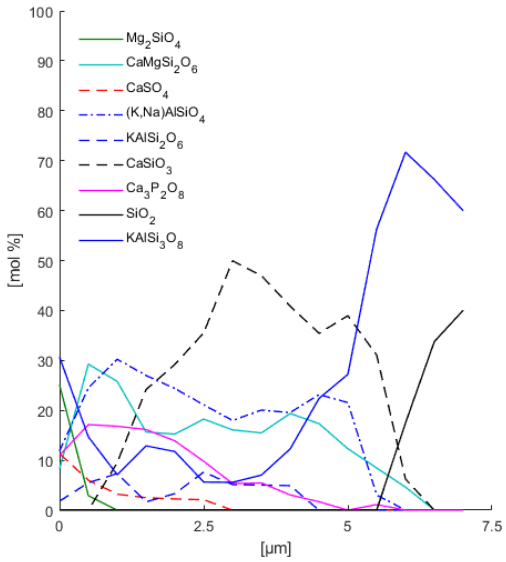

Figure 4.10: FactSage thermodynamic modelling results showing the predominant phases which are in equilibrium for the compositions measured with EDS.

Considering the change in Gibbs free energy due to the chemical reactions which can occur on the surface of the bed material, a number of reactions involve a decrease in Gibbs free energy, meaning they occur spontaneously. For the case of feldspar, the interaction of both types of feldspar with CaO is shown in Figure 4.11. Both Na- and K-feldspar can react with CaO to form $CaSiO_3$ and the respective SiO_2-reduced feldspathoid. This phase can undergo another reaction with CaO to form $CaSiO_3$ and the respective Na- or K-$AlSiO_4$ phase. However, the reaction between $KAlSiO_4$ and Na-feldspar is spontaneous as well, yielding K-feldspar and $NaAlSiO_4$. This can be interpreted as the explanation for the replacement of Na-feldspar by K-feldspar. While both phases can react with CaO, only K-feldspar can regenerate by consuming further Na-feldspar.

Similar reactions are possible with KOH, leading to the formation of K-silicates instead of $CaSiO_3$. Depending on ash composition, either CaO or KOH will be the major reaction partner for the feldspar. In both cases, the replacement of Na-feldspar by K-feldspar will be the outcome.

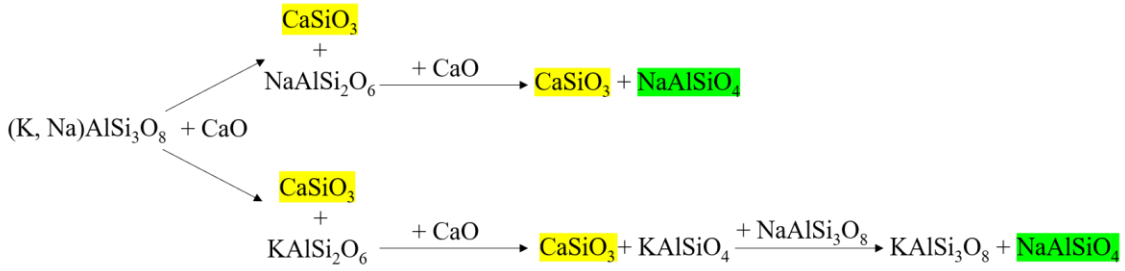

Figure 4.11: Suggested reactions associated with a decrease in Gibbs free energy, involving the two types of feldspar (K- and Na-) and CaO at 1123 K.

4.5 Minor Ash Elements

For further in-depth analysis, TEM analysis was conducted on the olivine sample extracted after 4 days retention time in the aging experiment. Therefore, a thin foil was extracted from one particle extracted after four days by focused ion beam milling and analyzed with TEM. The results are shown in Figure 4.12.

The previously described three layered structure is indicated in the micrograph, showing that the *surface layer* which is located in the first 400 nm consists mostly of Mg and Fe. Periclase (MgO), which was found in XRD, is the phase expected to be present in the *surface layer* and it can form a solid solution with minor amounts of FeO.[65] Due to the higher oxygen partial pressure on the surface of the particles, a migration of Fe^{2+} from the olivine structure towards the surface can be expected, where Fe^{2+} oxidizes to Fe^{3+}. Therefore, the formation of magnesioferrite ($MgFe_2O_4$) is possible, which could however not be found with XRD.

The *intermediate layer* spans from 400 nm to 3600 nm. In Figure 4.12, the layer is further subdivided into a dense outer layer which contains up to 80 at. % Si and a porous inner layer where the concentration of Si is lower. It is apparent from the TEM-EDS line-scan that high concentrations of Si and Ca are alternating with high concentrations of Mg and Fe. This is in line with the formation of (Mg,Fe)O or $MgFe_2O_4$ and a separate Ca-silicate phase. The presence of periclase was confirmed with electron diffraction on the location marked as “A”. Here, a pattern corresponding to crystal structure of periclase could be recorded. The lower porosity at locations high in Si could be interpreted as a filling up of pores with Si. Other phases detected in the *intermediate layer* are $CaTiO_3$, $Ca_3(PO_4)_2$ and $K_2Ca_2(SO_4)_3$ which were calculated with FactSage from the composition recorded at the respective points.

Between 3600 nm and 4700 nm, the *inner layer* is located, which is rich in Si and Ca except for the Mg and Fe rich precipitation at 4400 nm. The layer’s composition is about 80 at. % Si and 20 at. Ca which is a higher ratio of Si:Ca than expected for the suggested $CaMgSiO_4$. This could be caused by the formation of $MgFe_2O_4$ due to the oxidation of Fe^{2+} to Fe^{3+} which depletes the silicate structure of cations. A diffraction pattern recorded on the location indicated with “B”, showed the formation of an amorphous phase. The formation of amorphous silica has been found previously in oxidation experiments with olivine, where temperatures above 900 °C where necessary to form crystals of more polymerized silica structures.[66,67]

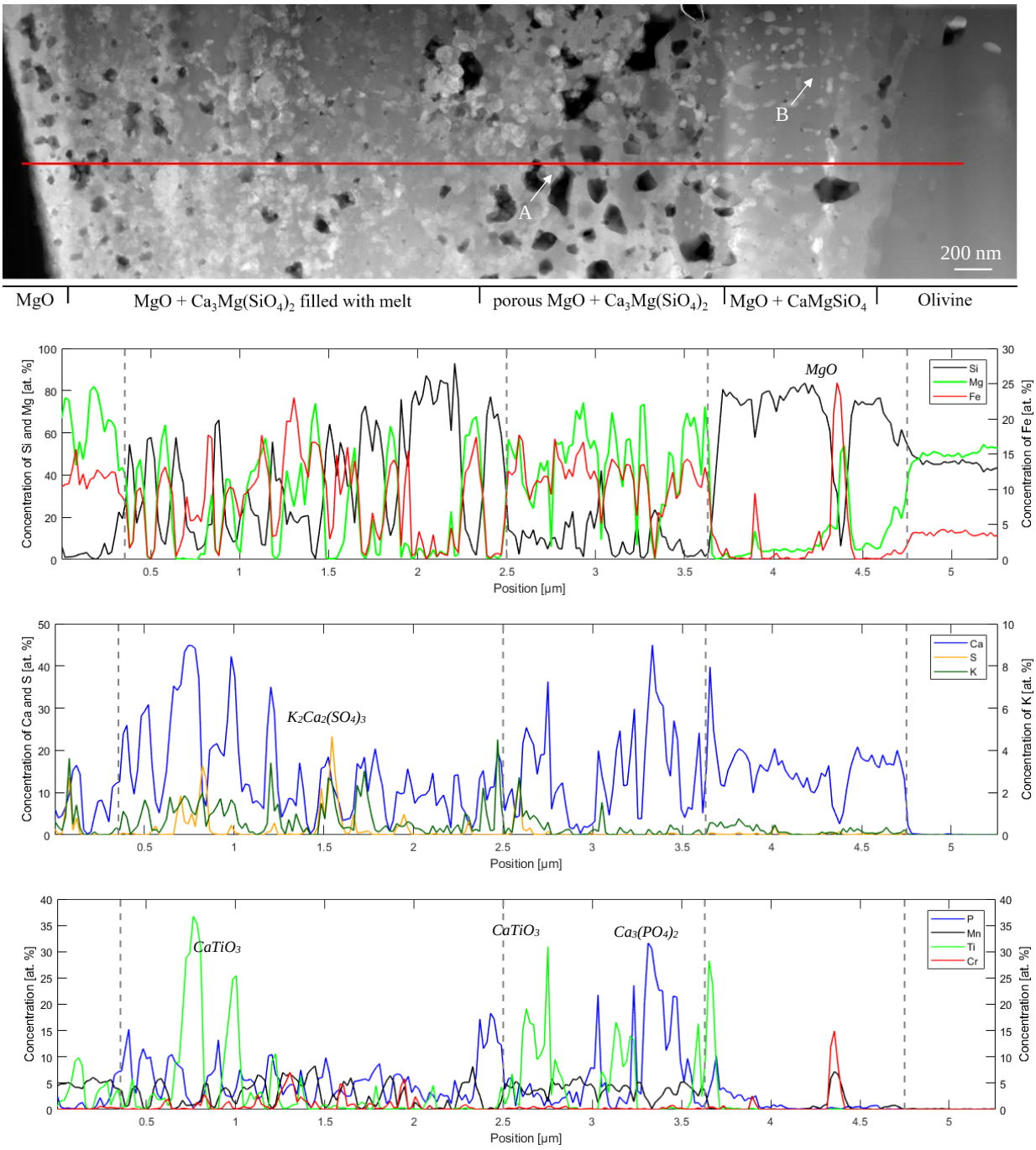

Figure 4.12: Micrograph of the TEM foil and EDS line-scans corresponding to the location indicated with the red line recorded on an olivine particle extracted after 4 days residence time in the aging experiment. A and B indicate the locations where the diffraction patterns were recorded. (top) elemental distribution of elements initially present in olivine: Si, Mg and Fe; (middle) elements suspected to increase the catalytic activity of the bed material: Ca, S and K; (bottom) other elements found in significant quantities: P, Mn, Ti and Cr.

4.6 Summary

4.6.1 Quartz

When utilizing quartz sand as bed material, the interaction can be summarized by the four steps shown in Figure 4.13. K, which is expected to be present as gaseous hydroxide can rapidly react with quartz to form K-silicate melt. The diffusion of K^+-ions can proceed faster than Ca^{2+} or Mg^{2+} due K^+ being single charged. Thus, the formation of K-silicate melt spreads faster than the formation of compounds containing other ash elements. Melt derived from SiO_2 exhibits a high degree of polymerization and has therefore a high viscosity (making it sticky) which explains the tendency of quartz bed material to agglomerate. Conversely, if ash derived CaO interacts with the K-silicate melt, the formation of $CaSiO_3$ occurs. This structure is solid at 850 °C and can therefore function as a cover for the melt which can decrease the agglomeration tendency. This effect is decreased in the presence of P which reacts with Ca to form $Ca_3(PO_4)_2$ which is deposited on the bed material. The interaction with Mg appears to be minor, as only (comparably) small amounts of Mg are found in biomass ash. Mg tends to react with $CaSiO_3$ forming the less polymerized nesosilicate $Ca_3Mg(SiO_4)_2$.

The analysis shows that the interaction of biomass ash with quartz bed particles leads to the accumulation of Ca, Mg and P on the surface. These elements could therefore be responsible for the increase in activity towards tar reduction which the bed material shows upon prolonged residence time in the gasifier. While quartz is generally considered inert, the accumulation of said elements leads to an activation of the particles, as long as severe agglomeration caused by the K-silicate melt can be avoided. Thus, the utilization of Ca- or Mg-rich fuel or additives could promote the formation of higher-melting Ca-Mg-silicates which can function as a protection against agglomeration, since the K-silicate melt is located underneath.

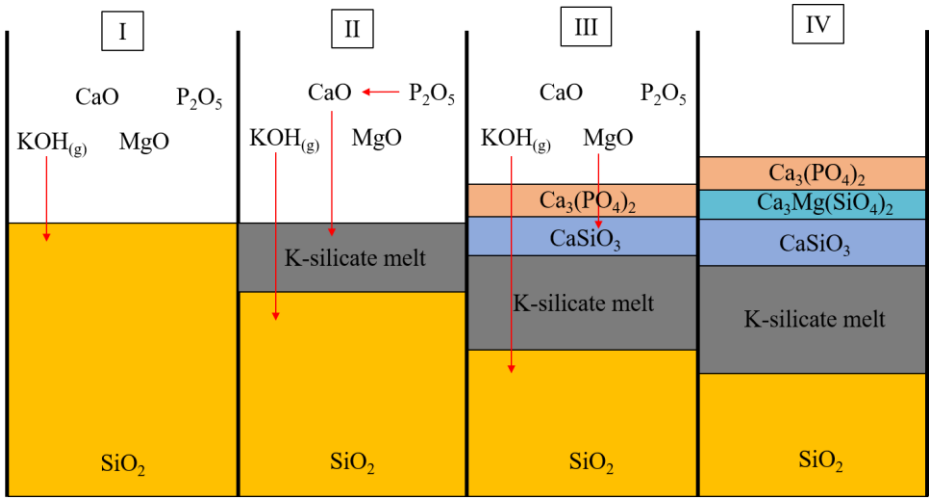

Figure 4.13: Schematic representation of the interaction of quartz sand with the major components of biomass ash.

4.6.2 Olivine

A schematic summary of the interaction of olivine with the main ash elements is shown in Figure 4.14. Contrary to quartz, KOH does not interact strongly with olivine which is why the first step is the reaction of CaO with olivine. Thereby, a mixed Ca-Mg-silicate is formed and MgO is expelled from the olivine structure. Ash-derived P is deposited as Ca-phosphate which limits the interaction potential of Ca with olivine. $CaMgSiO_4$ is expected as an intermediate Ca-Mg-silicate which will be replaced by $Ca_3Mg(SiO_4)_2$

on the surface due to further replacement with Ca. As the formed ash layer exhibits porosity, small amounts of a K-rich phase can be incorporated. Prolonged retention time of the particles leads to the formation of several alternating $Ca_3Mg(SiO_4)_2$/MgO layers.

In previous studies on olivine activation, Ca has often been speculated to be responsible for the increased activity of the bed material towards tar reduction. The analysis done in the present study show that a layer of MgO is present on the outer surface which is therefore the phase which is most likely in contact with the gas phase. To efficiently increase the activity of olivine bed material, the choice of fuel and additives should therefore be made to promote the formation of a MgO layer.

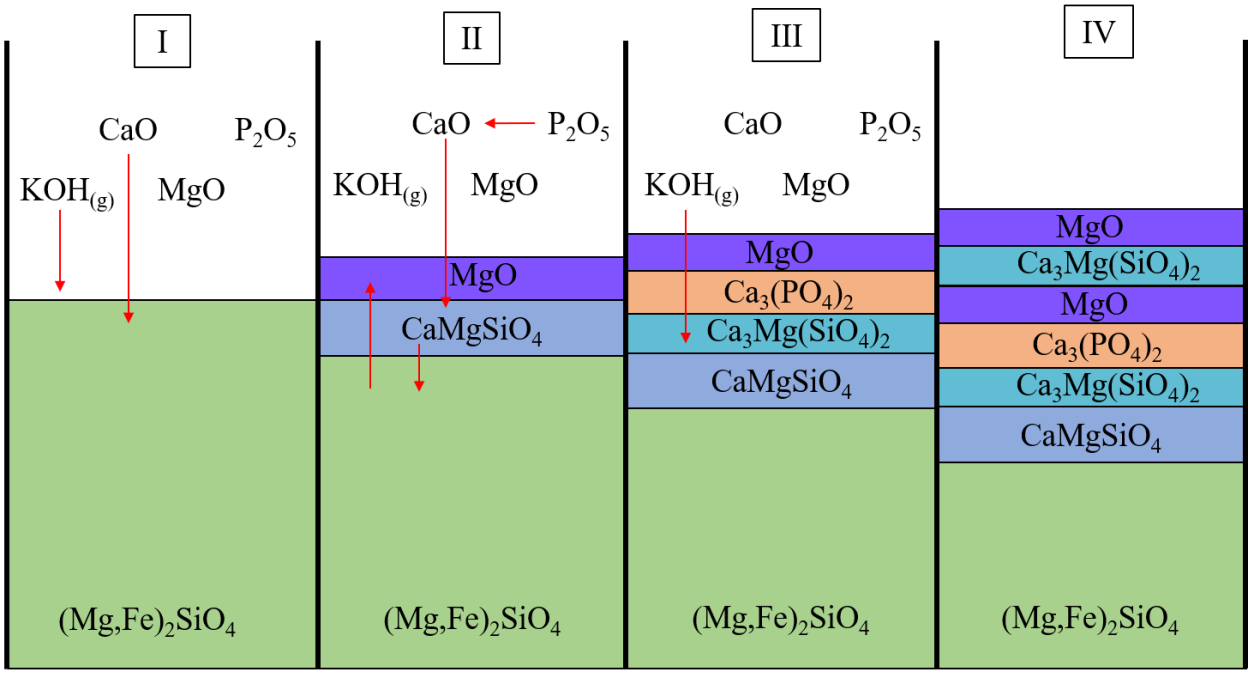

Figure 4.14: Schematic depiction of the interaction of the main ash elements with olivine.

4.6.3 **Feldspar**

The interaction of alkali-feldspar with biomass ash is schematically shown in Figure 4.15. The interaction of CaO with both types of feldspar leads to the formation of $CaSiO_3$ and Si-reduced feldspathoids. As the reaction of the $KAlSiO_4$ with Na-feldspar leads to the formation of $NaAlSiO_4$ and K-feldspar, eventually all Na-feldspar will be replaced by K-feldspar. This process is amplified by K-derived ash interacting the bed material. Conversely, the presence of P in biomass ash causes the deposition of $Ca_3(PO_4)_2$ which reduces the interaction potential of Ca with the bed material. Mg from the biomass ash can interact with $CaSiO_3$ to form $Ca_3Mg(SiO_4)_2$.

The depolymerization of the silicate network is similar to what was previously described for quartz; however, no detrimental melt formation was found. As an increase in activity towards tar reduction of alkali-feldspar bed material was found, a beneficial effect of depolymerizing the silicate network seems to exist. By utilizing feedstock rich in Ca and Mg, and poor in P, the depolymerization can be amplified which could reduce the residence time required for the bed material to achieve an active state.

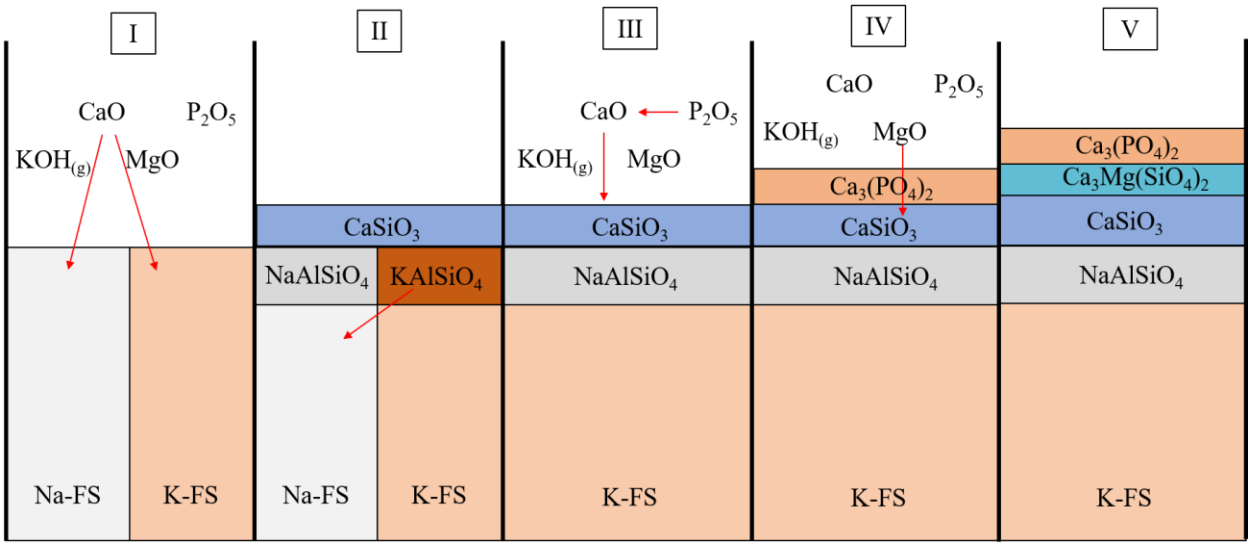

Figure 4.15: Schematic depiction of the interaction of biomass ash with alkali-feldspar.

5 Conclusion

The interaction of biomass ash with silicate bed material under gasification conditions was investigated on quartz, alkali-feldspar, and olivine. Prolonged residence time of the bed material particles causes the accumulation of ash-derived elements, of which the major elements are Mg, P, K and Ca. The accumulation of ash-derived Ca (and to a lesser extent Mg), causes the depolymerization of the silicate lattice of quartz and feldspar, as shown in Figure 5.1. This effect is reduced by the presence of P in the fuel ash which decreases the amount of Ca to react with the bed material by the formation of stable $Ca_3(PO_4)_2$. For the case of olivine, further depolymerization of the tectosilicate is not possible, which is why a replacement of Mg and Fe from the olivine lattice by Ca occurs. This leads to the formation of a MgO surface layer with small amounts of Fe.

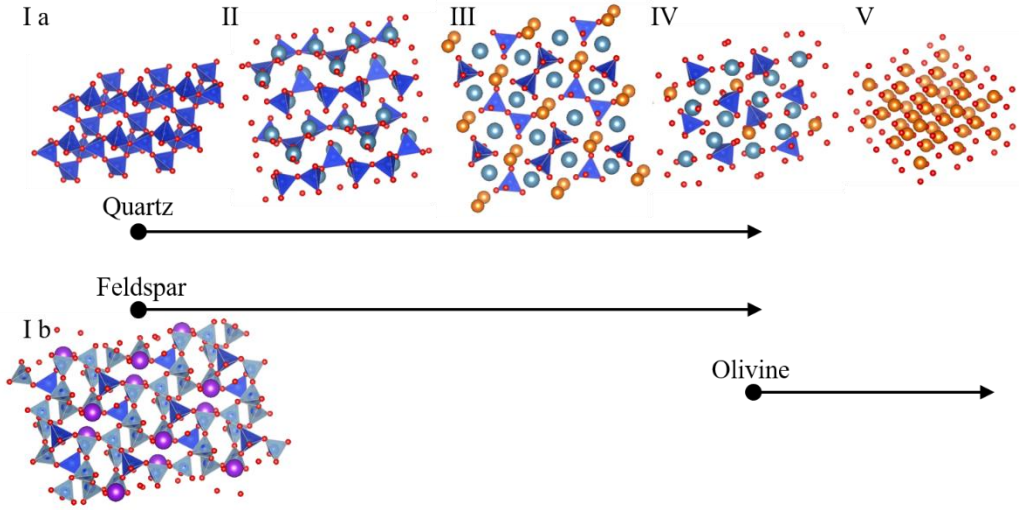

Figure 5.1: Schematic depiction of the general mechanism of structure change found for the three bed materials investigated. The structures shown are the tectosilicates quartz (I a) and K-feldspar (I b), the inosilicate wollastonite (II), the sorosilicate åkermanite (III), the nesosilicate merwinite (IV), and periclase (V). O: red, Si: inside the blue tetrahedrons, Ca: turquoise, Mg: orange, K: purple.[68]

For all investigated bed materials, the development of less polymerized silicate minerals was found at the same time as an increase in activity towards tar reduction was recorded. While these findings have strong implications towards possible active minerals, further studies are required to test the activity of the pure minerals, as other factors such as porosity might have an effect on the activity.

6 Future Work

This work provides an overview on how silicate bed materials interact with biomass ash. The results point on a beneficial effect of less polymerized silicate structures caused by increasing the concentration of Ca and Mg. Besides the chemical composition of the surface which can be altered by additives and ash interaction, factors such as morphology and porosity of the bed particles should be studied to further investigate the impact of surface area on the bed material's activity. Furthermore, the underlying mechanism for the catalytic activity of the bed material should be further investigated by measuring oxygen carrying ability or the release of active species from the material.

The choice of fuel is not only limited to biomass, but waste streams could be applied as an alternative. Since their ash composition differs from biomass, it is important to study whether the interactions are comparable to biomass and an increase in activation can be achieved following a similar pathway.

Furthermore, studies should be conducted to analyze the impact of additives, for example Ca-Mg-carbonates such as calcite, magnesite, or dolomite, in order to achieve an active state of the bed material without the requirement of prolonged retention time. Investigations on the impact of additives on the layer structure can aid to choose synergistic combinations of fuel, bed material, and additives. This knowledge can be used to apply these materials for other thermal conversion technologies, such as combustion of biomass.

7 Bibliography

1. IEA. Key world energy statistics. 101 (2019).
2. Intergovernmental Panel on Climate Change. *Climate Change 2014 Mitigation of Climate Change*. (2014). doi:10.1017/cbo9781107415416
3. Quéré, C. *et al.* Global Carbon Budget 2018. *Earth Syst. Sci. Data* **10**, 2141–2194 (2018).
4. Kirnbauer, F., Wilk, V., Kitzler, H., Kern, S. & Hofbauer, H. The positive effects of bed material coating on tar reduction in a dual fluidized bed gasifier. *Fuel* **95**, 553–562 (2012).
5. Bridgwater, A. V. The technical and economic feasibility of biomass gasification for power generation. *Fuel* **74**, 631–653 (1995).
6. Grassi, G. & Bridgwater, A. V. The european community energy from biomass research and development programme. *Int. J. Sol. Energy* **10**, 127–136 (1991).
7. Loppinet-Serani, A., Aymonier, C. & Cansell, F. Current and foreseeable applications of supercritical water for energy and the environment. *ChemSusChem* **1**, 486–503 (2008).
8. Lemus, R. & Lal, R. Bioenergy crops and carbon sequestration. *CRC. Crit. Rev. Plant Sci.* **24**, 1–21 (2005).
9. Zanchi, G., Pena, N. & Bird, N. Is woody bioenergy carbon neutral? A comparative assessment of emissions from consumption of woody bioenergy and fossil fuel. *GCB Bioenergy* **4**, 761–772 (2012).
10. Smeets, E. M. W. & Faaij, A. P. C. The impact of sustainability criteria on the costs and potentials of bioenergy production - Applied for case studies in Brazil and Ukraine. *Biomass and Bioenergy* **34**, 319–333 (2010).
11. Smeets, E. M. W. & Faaij, A. P. C. Bioenergy potentials from forestry in 2050: An assessment of the drivers that determine the potentials. *Clim. Change* **81**, 353–390 (2007).
12. Nijsen, M., Smeets, E., Stehfest, E. & van Vuuren, D. P. An evaluation of the global potential of bioenergy production on degraded lands. *GCB Bioenergy* **4**, 130–147 (2012).
13. Parikka, M. Global biomass fuel resources. *Biomass and Bioenergy* **27**, 613–620 (2004).
14. Van Camp, W. Yield enhancement genes: Seeds for growth. *Curr. Opin. Biotechnol.* **16**, 147–153 (2005).
15. Ragauskas, A. J. *et al.* The path forward for biofuels and biomaterials. *Science (80-.).* **311**, 484–489 (2006).
16. Malkow, T. Novel and innovative pyrolysis and gasification technologies for energy efficient and environmentally sound MSW disposal. *Waste Manag.* **24**, 53–79 (2004).
17. De Andrés, J. M., Narros, A. & Rodríguez, M. E. Behaviour of dolomite, olivine and alumina as primary catalysts in air-steam gasification of sewage sludge. *Fuel* **90**, 521–527 (2011).
18. Thunman, H. *et al.* Circular use of plastics-transformation of existing petrochemical clusters into thermochemical recycling plants with 100% plastics recovery. *Sustain. Mater. Technol.* **22**, e00124 (2019).
19. Larsson, A., Seemann, M., Neves, D. & Thunman, H. Evaluation of performance of industrial-scale

dual fluidized bed gasifiers using the chalmers 2-4-MWth gasifier. *Energy and Fuels* **27**, 6665–6680 (2013).

20. Xu, G., Murakami, T., Suda, T., Matsuzawa, Y. & Tani, H. The superior technical choice for dual fluidized bed gasification. *Ind. Eng. Chem. Res.* **45**, 2281–2286 (2006).

21. Murakami, T. *et al.* Some process fundamentals of biomass gasification in dual fluidized bed. *Fuel* **86**, 244–255 (2007).

22. Marinkovic, J. Choice of bed material: a critical parameter in the optimization of dual fluidized bed systems. (PhD Thesis, Chalmers University of Technology, 2016).

23. Bridgwater, A. V. Renewable fuels and chemicals by thermal processing of biomass. *Chem. Eng. J.* **91**, 87–102 (2003).

24. Karl, J. & Pröll, T. Steam gasification of biomass in dual fluidized bed gasifiers: A review. *Renew. Sustain. Energy Rev.* **98**, 64–78 (2018).

25. Kirnbauer, F., Wilk, V. & Hofbauer, H. Performance improvement of dual fluidized bed gasifiers by temperature reduction: The behavior of tar species in the product gas. *Fuel* **108**, 534–542 (2013).

26. Devi, L., Ptasinski, K. J. & Janssen, F. J. J. G. A review of the primary measures for tar elimination in biomass gasification processes. *Biomass and Bioenergy* **24**, 125–140 (2002).

27. Larsson, A., Gunnarsson, I. & Tengberg, F. The GoBiGas Project. 52 (2018).

28. De Lasa, H., Salaices, E., Mazumder, J. & Lucky, R. Catalytic steam gasification of biomass: Catalysts, thermodynamics and kinetics. *Chem. Rev.* **111**, 5404–5433 (2011).

29. Milne, T. A., Evans, R. J. & Abatzaglou, N. Biomass Gasifier '"Tars"': Their Nature, Formation, and Conversion. (1998). doi:10.2172/3726

30. Berdugo Vilches, T. *et al.* Bed material as a catalyst for char gasification: The case of ash-coated olivine activated by K and S addition. *Fuel* **224**, 85–93 (2018).

31. Koppatz, S., Pfeifer, C. & Hofbauer, H. Comparison of the performance behaviour of silica sand and olivine in a dual fluidised bed reactor system for steam gasification of biomass at pilot plant scale. *Chem. Eng. J.* **175**, 468–483 (2011).

32. Mauerhofer, A. M. *et al.* Influence of different bed material mixtures on dual fluidized bed steam gasification. *Energy* **157**, 957–968 (2018).

33. Berdugo Vilches, T., Marinkovic, J., Seemann, M. & Thunman, H. Comparing Active Bed Materials in a Dual Fluidized Bed Biomass Gasifier: Olivine, Bauxite, Quartz-Sand, and Ilmenite. *Energy and Fuels* **30**, 4848–4857 (2016).

34. Devi, L., Craje, M., Thüne, P., Ptasinski, K. J. & Janssen, F. J. J. G. Olivine as tar removal catalyst for biomass gasifiers: Catalyst characterization. *Appl. Catal. A Gen.* **294**, 68–79 (2005).

35. Kurkela, E., Kurkela, M. & Hiltunen, I. Steam-oxygen gasification of forest residues and bark followed by hot gas filtration and catalytic reforming of tars: Results of an extended time test. *Fuel Process. Technol.* **141**, 148–158 (2016).

36. Berguerand, N., Marinkovic, J., Berdugo Vilches, T. & Thunman, H. Use of alkali-feldspar as bed material for upgrading a biomass-derived producer gas from a gasifier. *Chem. Eng. J.* **295**, 80–91 (2016).

37. Zevenhoven-Onderwater, M., Backman, R., Skrifvars, B.-J. & Hupa, M. The ash chemistry in fluidised bed gasification of biomass fuels. Part I: predicting the chemistry of melting ashes and ash–bed material interaction. *Fuel* **80**, 1489–1502 (2001).

38. Zevenhoven, M., Yrjas, P., Skrifvars, B. J. & Hupa, M. Characterization of ash-forming matter in various solid fuels by selective leaching and its implications for fluidized-bed combustion. *Energy and Fuels* **26**, 6366–6386 (2012).

39. Vassilev, S. V, Baxter, D. & Vassileva, C. G. An overview of the behaviour of biomass during combustion: Part II. Ash fusion and ash formation mechanisms of biomass types. *Fuel* **117**, 152–183 (2013).

40. Berdugo Vilches, T. Operational strategies to control the gas composition in dual fluidized bed biomass gasifiers. (Chalmers, 2018).

41. Öhman, M., Pommer, L. & Nordin, A. Bed agglomeration characteristics and mechanisms during gasification and combustion of biomass fuels. *Energy and Fuels* **19**, 1742–1748 (2005).

42. Brus, E., Öhman, M. & Nordin, A. Mechanisms of bed agglomeration during fluidized-bed combustion of biomass fuels. *Energy and Fuels* **19**, 825–832 (2005).

43. Brus, E. *et al.* Bed agglomeration characteristics of biomass fuels using blast-furnace slag as bed material. *Energy and Fuels* **18**, 1187–1193 (2004).

44. Grimm, A., Skoglund, N., Boström, D. & Öhman, M. Bed agglomeration characteristics in fluidized quartz bed combustion of phosphorus-rich biomass fuels. *Energy and Fuels* **25**, 937–947 (2011).

45. Zevenhoven-Onderwater, M., Backman, R., Skrifvars, B. J. & Hupa, M. The ash chemistry in fluidised bed gasification of biomass fuels. Part II: Ash behaviour prediction versus bench scale agglomeration tests. *Fuel* **80**, 1503–1512 (2001).

46. Fryda, L. E., Panopoulos, K. D. & Kakaras, E. Agglomeration in fluidised bed gasification of biomass. *Powder Technol.* **181**, 307–320 (2008).

47. Zhou, C., Rosén, C. & Engvall, K. Biomass oxygen/steam gasification in a pressurized bubbling fluidized bed: Agglomeration behavior. *Appl. Energy* **172**, 230–250 (2016).

48. Liliedahl, T., Sjöström, K., Engvall, K. & Rosén, C. Defluidisation of fluidised beds during gasification of biomass. *Biomass and Bioenergy* **35**, 3–10 (2011).

49. Meng, X., de Jong, W., Fu, N. & Verkooijen, A. H. M. Biomass gasification in a 100 kWth steam-oxygen blown circulating fluidized bed gasifier: Effects of operational conditions on product gas distribution and tar formation. *Biomass and Bioenergy* **35**, 2910–2924 (2011).

50. Kuba, M. *et al.* Thermal Stability of Bed Particle Layers on Naturally Occurring Minerals from Dual Fluid Bed Gasification of Woody Biomass. *Energy and Fuels* **30**, 8277–8285 (2016).

51. Kuo, J. H., Lin, C. L. & Wey, M. Y. Effect of alkali concentrations and operating conditions on agglomeration/defluidization behavior during fluidized bed air gasification. *Powder Technol.* **214**, 443–446 (2011).

52. Bale, C. W. *et al.* FactSage Thermochemical Software and Databases, 2010-2016 - FTDemo Database. *Calphad* **54**, 35–53 (2016).

53. Rapagnà, S., Jand, N., Kiennemann, A. & Foscolo, P. U. Steam-gasification of biomass in a fluidised-bed of olivine particles. *Biomass and Bioenergy* **19**, 187–197 (2000).

54. Marinkovic, J., Thunman, H., Knutsson, P. & Seemann, M. Characteristics of olivine as a bed material in an indirect biomass gasifier. *Chem. Eng. J.* **279**, 555–566 (2015).

55. Kuba, M. *et al.* Deposit build-up and ash behavior in dual fluid bed steam gasification of logging residues in an industrial power plant. *Fuel Process. Technol.* **139**, 33–41 (2015).

56. Kirnbauer, F. & Hofbauer, H. Investigations on bed material changes in a dual fluidized bed steam gasification plant in Güssing, Austria. *Energy and Fuels* **25**, 3793–3798 (2011).

57. Kuba, M., Kirnbauer, F. & Hofbauer, H. Influence of coated olivine on the conversion of intermediate products from decomposition of biomass tars during gasification. *Biomass Convers. Biorefinery* **7**, 11–21 (2017).

58. Kirnbauer, F. & Hofbauer, H. The mechanism of bed material coating in dual fluidized bed biomass steam gasification plants and its impact on plant optimization. *Powder Technol.* **245**, 94–104 (2013).

59. Knutsson, P., Cantatore, V., Seemann, M., Tam, P. L. & Panas, I. Role of potassium in the enhancement of the catalytic activity of calcium oxide towards tar reduction. *Appl. Catal. B Environ.* **229**, 88–95 (2018).

60. Kuba, M. *et al.* Mechanism of layer formation on olivine bed particles in industrial-scale dual fluid bed gasification of wood. *Energy and Fuels* **30**, 7410–7418 (2016).

61. Schreiber, H. D. Experimental studies of nickel and chromium partitioning into olivine from synthetic basaltic melts. *Proc. Lunar Planet. Sci. Conf.* (1979).

62. Berguerand, N. & Berdugo Vilches, T. Alkali-Feldspar as a Catalyst for Biomass Gasification in a 2-MW Indirect Gasifier. *Energy and Fuels* **31**, 1583–1592 (2017).

63. Wagner, K., Hammerl, C., Kuba, M. & Hofbauer, H. Time-Dependent Catalytic Activation of Inactive K-Feldspar by Layer Formation during Fluidized Bed Conversion with Residual Fuels. *27th Eur. Biomass Conf. Exhib.* 681–683 (2019).

64. He, H., Skoglund, N. & Öhman, M. Time-Dependent Layer Formation on K-Feldspar Bed Particles during Fluidized Bed Combustion of Woody Fuels. *Energy and Fuels* **31**, 12848–12856 (2017).

65. Geiger, C. A. *Solid Solutions in Silicate and Oxide systems*. (The Mineralogical Society of Great Britain and Ireland, 2001).

66. McKernan, S. & Carter, C. B. The Growth of Hematite by Oxidation of Iron-bearing Olivine. *Ultramicroscopy* **30**, 256–262 (1989).

67. Świerczyński, D., Courson, C., Bedel, L., Kiennemann, A. & Vilminot, S. Oxidation reduction behavior of iron-bearing olivines (Fe xMg1-x)2SiO4 used as catalysts for biomass gasification. *Chem. Mater.* **18**, 897–905 (2006).

68. Mommaa, K. & Izumia, F. VESTA 3 for three-dimensional visualization of crystal, volumetric and morphology data. *J. Appl. Crystallogr.* **44**, 1272–1276 (2011).